REPORT DOCUMENTATION PAGE

Form Approved
OMB No. 0704-0188

1. AGENCY USE ONLY *(Leave blank)*	2. REPORT DATE	3. REPORT TYPE AND DATES COVERED
	26 June 1999	Final, 10 Mar 97 - 28 May 98

4. TITLE AND SUBTITLE
Advanced Characterization of Photonic Materials for Volumetric 3-D Displays

5. FUNDING NUMBERS
G N000149710359

6. AUTHOR(S)
Richard E. Riman

7. PERFORMING ORGANIZATION NAME(S) AND ADDRESS(ES)
Rutgers, the State University of New Jersey
Department of Ceramic and Materials Engineering
607 Taylor Road
Piscataway, NJ 08854

8. PERFORMING ORGANIZATION REPORT NUMBER
Not Applicable

9. SPONSORING / MONITORING AGENCY NAME(S) AND ADDRESS(ES)
Office of Naval Research, Code 1141SB
800 N. Quincy Street
Arlington, VA 22217

10. SPONSORING / MONITORING AGENCY REPORT NUMBER
Not Applicable

11. SUPPLEMENTARY NOTES
None

12a. DISTRIBUTION / AVAILABILITY STATEMENT
Distribution Unlimited

12b. DISTRIBUTION CODE

13. ABSTRACT *(Maximum 200 words)*

A spectrometer was built that can measure various types of luminscence at a spectrum of infrared and visible wavelengths. The system is capable of fluorescence, lifetime and quantum efficiency measurements for single and two-step upconversion studies. Samples in the form of powders, liquid and monolithic solids can be examined.

In conclusion, current optical spectroscopy hardware can be implemented cost effectively. Furthermore, this equipment is very useful for developing materials for flat panel and volumetric displays.

14. SUBJECT TERMS
Displays, Flat Panel Displays, Volumetric Displays, Luminscence, Fluorescence, Photonic Materials

15. NUMBER OF PAGES
2

16. PRICE CODE

17. SECURITY CLASSIFICATION OF REPORT	18. SECURITY CLASSIFICATION OF THIS PAGE	19. SECURITY CLASSIFICATION OF ABSTRACT	20. LIMITATION OF ABSTRACT
Unclassified	Unclassified	Unclassified	SAR

FINAL REPORT

Grant #: N000149710359

PRINCIPAL INVESTIGATOR: Dr. Richard E. Riman

INSTITUTION: Rutgers University

GRANT TITLE: Advanced Characterization of Photonic Materials for Volumetric 3-D Displays

AWARD PERIOD: 3/10/97 - 5/28/98

OBJECTIVE: Build a spectrometer that can measure various types of luminescence at a spectrum of infrared and visible wavelengths.

APPROACH: Six configurations were evaluated in three areas: I. Ability to accommodate solids (monolithic and particulates), liquids, and suspensions. II. Capability of measuring luminescence (single and two stage), e-folding times, and quantum efficiencies. III. Flexibility in excitation (IR) and detection wavelengths (VIS and IR). Performance was optimized to meet our cost goals. Only one instrumentation configuration could meet that goal.

ACCOMPLISHMENTS: We have designed and implemented an optical characterization lab, which we feel provides us with the best performance and highest flexibility possible. The system that we have pieced together incorporates an optical characterization setup with previously unattainable capabilities. The system is capable of fluorescence, lifetime, and quantum efficiency measurements for one-step and two-step, two-frequency upconversion studies. We have the capability of characterizing solids, powders, and liquids.

The use of two laser diode head units allows for optical pumping of samples with two different wavelengths of light. Diodes of any wavelength can be installed in either unit to provide us with lasing at any wavelength a diode exists. Currently we have five different diodes (810, 855, 980, 1014, 1120 nm) which allows for upconversion of the rare-earth ions (namely, Er, Tm, Pr, Yb) of interest.

Our system is fully integrated into a software package which allows for computer controlled data sampling. Data can be obtained, manipulated, examined, and saved simultaneously. This allows for an large amount of experiments in a short time. The computer also allows for monitoring of the system to pinpoint any problems. Calibrated light sources allow constant monitoring of equipment performance.

CONCLUSIONS: Current optical spectroscopy hardware can be implemented very cost-effectively to meet a broad range of performance requirements that was not possible just a few years ago.

SIGNIFICANCE: We have a state of the art spectrometer that can evaluate luminescent materials useful for flat panel and volumetric displays. It is also practical in characterizing materials for optical communications.

PATENT INFORMATION: None.

AWARD INFORMATION: Our new capability in luminescent spectroscopy has successfully led to a research program funded by Dupont de Nemours, Inc.. The work will begin this July.

PUBLICATIONS AND ABSTRACTS:

J. Ballato, R. E. Riman, and E. Snitzer, "Highly Efficient 1.3 μm Luminescence from Rare-earth-doped Halides Prepared from Low Temperature Aqueous Solutions," *Optics & Photonics News,* December (1998) 17-18.

I-C. Lin, A. Navrotsky, J. Ballato, and R. E. Riman, "High Temperature Calorimetric Study of Glass-Forming Fluorozirconates," *J. Noncryst. Solids,* **215** (1997) 113.124.

J. Ballato, R. van Weeren, M. Agarwala, R. E. Riman, and S. C. Danforth, "Patterning for Planar Waveguides," *Electronics Letters,* **33** [1] (1997) 83-84.

J. Ballato, R. E. Riman, and E. Snitzer, "Sol-Gel Synthesis of Rare Earth-Doped Lanthanum Halides for Highly Efficient 1.3 μm Optical Amplification, " *Optics Letters,* **22** [10] (1997) 691-693.

J. Ballato, R. E. Riman, and E. Snitzer, "Sol-Gel Synthesis of Fluoride Optical Materials for Planar Integrated Photonic Applications," *J. Noncryst. Solids,* **213 & 214** (1997) 126-136.

J. Ballato, R. E. Riman, and E. Snitzer, "Sol-Gel Synthesis of Rare-Earth-Doped Lanthanum Halides for Highly Efficient Optical Amplification," Optical Society of America - Optical Amplifiers and Their Applications Topical Meeting, Victoria, B. C., Canada, July 21-23, 1997.

J. Ballato, R. E. Riman, and E. Snitzer, "Luminescent Behavior of Sol-Gel-Derived Pr^{3+} and Dy^{3+} Doped Lanthanum Halides for 1.3μm Optical Amplification," 99th Annual Meeting of the American Ceramic Society, Cincinnati, OH. May 4-7, 1997

J. Ballato, R. E. Riman, and E. Snitzer, "Sol-Gel Synthesis of Rare-Earth-Doped Lanthanum Halides for Highly Efficient 1.3 μm Optical Amplification,", 99th Annual Meeting of the American Ceramic Society, Cincinnati, OH. May 4-7, 1997.

J. Ballato, J. Plewa, R. E. Riman, and E. Snitzer, "Sol-Gel Synthesis of Multicomponent Fluoride Glasses," 99th Annual Meeting of the American Ceramic Society, Cincinnati, OH, May 4-7, 1997.

C. Haines, J. Ballato, and R. E. Riman, "Fluoride Fibers by Sol-Gel Core Deposition," 99th Annual Meeting of the American Ceramic Society, Cincinnati, OH, May 4-7, 1997.

Optical Amplifiers & Their Application

Sol-Gel Synthesis of Rare-Earth-Doped Lanthanum Halides For Highly Efficient Optical Amplification

John Ballato, Richard E. Riman, and Elias Snitzer

Rutgers, The State University of New Jersey
Fiber Optic Materials Research Program
Brett and Bowser Roads, Piscataway, NJ 08855-0909 USA
phone: (908) 445-4946, fax: (908) 445-6264

There exists a tremendous growth in photonic materials and device research as a result of both the explosion in telecommunications as well as the expected traffic requirements needed for interactive video and multimedia services. Economic perceptions regarding all-optical transmission systems were not nearly as favorable until the erbium doped fiber amplifier (EDFA) became a practical device to provide efficient, low-noise, broad-band gain for the 1.55 μm minimum-loss window.[1] The result is a global optical-amplifier market expected to be worth nearly $1.2 billion/year by 2004,[2] despite the fact that EDFAs are not appropriate for operation at the 1.3 μm zero-dispersion window that dominates existing fiber communications. For these reasons, there exists an international search for materials suitable for 1.3 μm optical amplification.

These optical amplifiers utilize Pr^{3+} or Dy^{3+} dopants to luminescence, and provide gain,[3,4] at 1.3 μm. Praseodymium (Pr^{3+}) has been the more aggressively studied and has reached some level of commercialization[5] despite the low quantum yield from current hosts. Dysprosium (Dy^{3+}) more recently has attracted interest since its absorption cross-section is significantly larger than Pr^{3+} and would greatly lessen the requisite amplifier length. Radiative transitions between rare-earth excited states are more efficient when host phonon energies are minimized. Toward this end, we considered the synthesis of doped-lanthanum halides. Material advantages with respect to silicate and chalcogenide hosts are reduced phonon energies (e.g., $\hbar\omega_{SiO_2}$ = 1100 cm^{-1} $\hbar\omega_{As_2S_3}$ = 350 cm^{-1}, $\hbar\omega_{LaF_3}$ = 350 cm^{-1}, $\hbar\omega_{LaCl_3}$ = 260 cm^{-1}), and very high solubilities for rare-earth dopants. The latter advantage allows for large sensitizing concentrations while maintaining an optimum luminescent dopant concentration. Further, a sol-gel approach to synthesis allows for greater ease and flexibility than achievable by conventional crystal-growing, or melt-quench (for glasses) techniques.

This work describes the synthesis and luminescent properties of Pr^{3+} and Dy^{3+} doped lanthanum halide powders by a sol-gel approach coupled with reactive atmosphere processing. Luminescence spectra and fluorescence lifetimes for the respective 1.3 μm transitions of these dopants are given and discussed in reference to melt-derived, single-crystal analogs.

Experimental Procedure

The synthesis of the lanthanum halides was accomplished by a two-step process. First, $LaCl_3 \cdot 6H_2O$ was dissolved in triply-deionized (DDD) water. Doped samples were synthesized by the addition of $PrCl_3 \cdot 6H_2O$ or $DyCl_3 \cdot 6H_2O$ to the aqueous $LaCl_3$ solution. Excess NH_4OH was added to precipitate $La(OH)_3$ out of solution. These samples subsequently were washed in DDD

water to remove the ammonium chloride reaction by-product, and dried at 90 °C for 24 hours. Secondly, the samples were transferred to an alumina muffle-tube furnace for reactive atmosphere processing. The sealed furnace was purged with nitrogen gas (liquid nitrogen source) and heated to temperature at 10 °C/min. Anhydrous hydrogen fluoride or hydrogen chloride (both 99.9 % pure) was subsequently introduced into the nitrogen flow providing conversion of the lanthanum hydroxide to the respective lanthanum halide (~ 500 cm^3/min HF or HCl, ~ 500 cm^3/min N_2). Reactive atmosphere processing lasted 1 hour, at which point the reactive gas was turned off and the furnace cooled to room temperature under flowing nitrogen. X-ray diffraction analysis was performed using Ni-filtered CuK_α radiation. Fluorescence measurements utilized a tunable Ti-sapphire laser excited by an argon-ion laser, which was chopped at 40 Hz. Luminescence spectra were measured with an InGaAs detector.

RESULTS

Sol-gel-derived Pr^{3+}- and Dy^{3+}-doped LaF_3 and $LaCl_3$ were produced successfully by a reactive atmosphere treatments of hydroxide powders. X-ray diffraction standards[6] were used to verify synthesis of the respective halides.

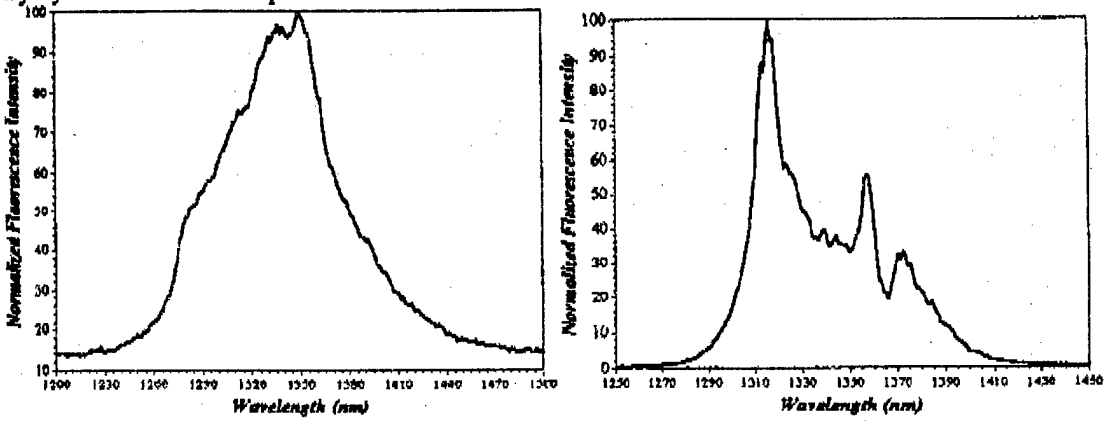

Figure 1. Normalized fluorescence spectra for sol-gel-derived LaF_3 doped with 750 ppm Pr^{3+} (left) and $LaCl_3$ doped with 500 ppm Pr^{3+} (right). Excitation for both occured at 1.017 μm using a Ar^+-pumped, $Ti:Al_2O_3$ laser.

Fluorescence at 1.3 μm from a 750 ppm Pr^{3+}-doped LaF_3 sample is presented in Figure 1. The 3 dB bandwidth is approximately 100 nm (1280 nm → 1380 nm) with peak asymmetry attributed to crystal-field effects. The lifetime for this emission was 0.23 milliseconds (Table 1). Figure 1 also shows the fluorescent emission at 1.3 μm from a 500 ppm Pr^{3+}-doped $LaCl_3$ sample. The effects of crystal-field symmetry clearly are evident with a maximum peak intensity occurring at about 1315 nm. The emission, although spectrally uneven, is broad-band ranging from 1290 nm to 1400 nm. Lifetimes for the chlorinated samples (Table 1) were on the order of 1 millisecond with a slight increase if chlorination occurred at a higher temperature.

Luminescence from the $(^6H_{9/2},^6F_{11/2}) \rightarrow {}^6H_{15/2}$ transition of Dy^{3+}:$LaCl_3$ (500 ppm) is shown in Figure 2. A 45 nm (1295 nm → 1345 nm) 3 dB bandwidth is observed with a characteristic three-peak spectral feature.[7] Radiative lifetimes for the 500 ppm samples were greater then 1.1 msec, again increasing with increased processing temperature.

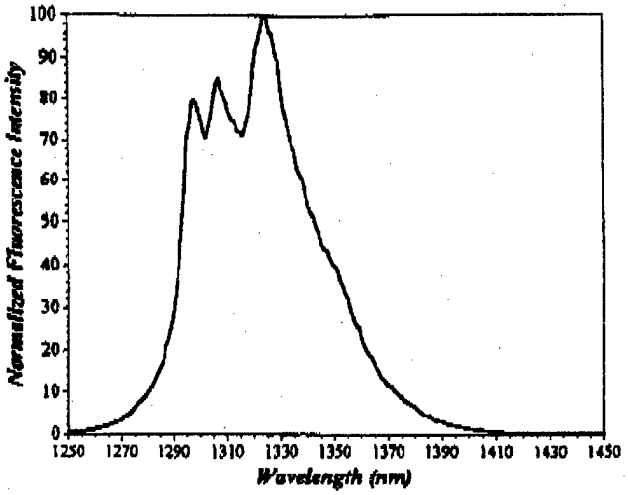

Figure 2. Normalized fluorescence spectra for sol-gel-derived $LaCl_3$ doped with 500 ppm Dy^{3+}. Excitation at 810 nm using a Ar^+-pumped, $Ti:Al_2O_3$ laser.

Determination of Radiative Quantum Efficiencies

The radiative quantum efficiency from the $^1G_4$ level of Pr^{3+} : LaF_3 may be determined by comparing the 0.23 msec measured lifetime (750 ppm Pr^{3+} : LaF_3 via sol-gel) to that calculated by Weber[8] following Judd-Ofelt analysis of Pr^{3+}-doped LaF_3 single crystals. In this case, the quantum efficiency is $\eta = \frac{\tau_{LaF_3}}{\tau_c} = \frac{0.23}{3.11} \cong 8\%$ where the 0.23 msec (τ_{LaF_3}) is the measured lifetime of the 1.3 μm emission from the HF600 sample and the 3.11 msec theoretical lifetime (τ_c) is the reciprocal of the $\Sigma A(^1G_4, J_j)$ value given by *Weber*.[8] This is approximately one-half the theoretical efficiency calculated from tabulated spontaneous emission probabilities and multiphonon emission rates. Absorbed OH is known to quench the $^1G_4$ lifetime,[9] therefore it is likely that this accounts for the less-than-theoretical quantum efficiency value as samples had not been isolated from the atmosphere.

The 260 cm^{-1} phonon energy of $LaCl_3$ infers an extremely low nonradiative relaxation rate and, hence, a potential radiative quantum efficiency of 100 % from the $^1G_4$ level. The lifetimes measured for this host correspond to an efficiency of $\eta = \frac{\tau_o}{\tau_c} = \frac{1.06}{1.466} = 72\%$. The 1.466 msec theoretical lifetime was calculated from the electric and magnetic dipole radiative rated following Judd-Ofelt analysis on Bridgeman-Stockbarger grown Pr^{3+}:$LaCl_3$ single crystals.

The spectroscopic properties of the sol-gel-derived, Dy-doped $LaCl_3$ samples with respect to melt-grown, single crystals[10]are in very close agreement. Radiative lifetimes for the Bridgeman-grown samples of Ref. 10 are on the order of 1.19 msec at room temperature, corresponding to a quantum efficiency of 68 %.[7] In comparison, the HF400 samples exhibited radiative lifetimes of 1.3 msec inferring an efficiency near 78 %.

TABLE 1. Measured lifetimes of 1.3 μm emission. The measured lifetimes correspond to when the luminescence intensity drops by exp (-1).

SAMPLE	MEASURED LIFETIME (msec)	QUANTUM EFFICIENCY (%)
750 ppm Pr:LaF_3 HF600[†]	0.23	8
500 ppm Pr:$LaCl_3$ HCl200	0.97	66
500 ppm Pr:$LaCl_3$ HCl400	1.06	72
500 ppm Dy:$LaCl_3$ HCl200	1.11	68
500 ppm Dy:$LaCl_3$ HCl400	1.31	78

[†] *Notation*: Abbreviation indicates halide gas and temperature; e.g., HF600 corresponds to anhydrous HF gas at 600 °C. All treatments lasted for 1 hour.

CONCLUSION

Highly efficient luminescence at 1.3 μm has been observed for the first time from sol-gel-derived materials. Comparison of these hosts to doped single crystals indicates equivalent spectroscopic performance. The versatility, ease, and low-cost of this sol-gel process represents a significant advance in 1.3 μm fluorescent materials for both optical fiber amplifiers and thin-film amplifiers for planar integrated photonics.

REFERENCES

1 C. A. Brackett, *J. Lightwave Technol.*, **14**, 986-941 (1996).

2 "Fiberoptics Industry Report," *Laser Focus World*, January 1996, p. 43.

3 Y. Ohishi, T. Kanamori, T. Kitagawa, S. Takahashi, E. Snitzer, and G. H. Sigel, Jr., *Optics Lett.*, **16**, 1747-1749 (1991).

4 D. W. Hewak, B. N. Samson, J. A. Mederios Neto, R. I. Laming, and D. N. Payne, *Electron. Lett.*, **30**, 968-970 (1994); K. Wei, D. Machewirth, J. Wenzel, E. Snitzer, and G. H. Sigel, Jr, *Optics Lett.*, **19**, 904-906 (1994).

5 T. J. Whitley, *J. Lightwave Technol.*, **13**, 744-760 (1995).

6 Joint Committee on Powder Diffraction Standards (JCPDS): 8-461 (LaF_3) and 12-605 ($LaCl_3$).

7 R. H. Page, K. I. Schaffers, G. D. Wilke, P. A. Waide, J. B. Tassano, R. J. Beach, and S. Payne, *OFC '96 Tech. Digest*, paper TuG2, 28 (1996).

8 M. J. Weber, *J. Chem. Phys.*, **48**, 4774-4780 (1968).

9 J. Faber, D. R. Simons, Y. Yan, and H. deWaal, *Proceedings of the SPIE*, vol. 2290, 80-88 (1994).

10 R. H. Page, K. I. Scaffers, S. A. Payne, and W. F. Krupke, submitted *J. Lightwave Technol.*

ELSEVIER

Journal of Non-Crystalline Solids 213&214 (1997) 126–136

JOURNAL OF NON-CRYSTALLINE SOLIDS

Sol–gel synthesis of fluoride optical materials for planar integrated photonic applications

John Ballato, Richard E. Riman *, Elias Snitzer

Fiber Optic Materials Research Program, Rutgers, The State University of New Jersey, Brett and Bowser Roads, Piscataway, NJ 08855-0909, USA

Abstract

The sol–gel synthesis of fluoride materials provides a viable and low-cost method for achieving planar and bulk devices for integrated photonic applications. This paper describes these prospects and methods for the experimental development of patterned and waveguiding films. The sol–gel synthesis from both metal-organic and inorganic precursor systems is discussed in relation to their potential for passive and active device applications.

1. Introduction

Hopes of bringing to the commercial, industrial, and military user, a communications system with larger information capacities, see for example [1], at greater rates, serve as an impetus to expand our knowledge on the processing of photonic materials. Planar waveguide geometries will play a significant role in future photonic devices. In an analogous manner to their electronic counterparts, integration of optical circuits increases functionality with fewer components and a reduced power consumption. In light of these benefits, optoelectronic integration has been likened to the creation of the transistor in terms of its technological significance [2]. Consequently, applications abound for both active (e.g., optical amplifiers, see for example [3], and novel laser glasses [4]) and passive devices (e.g., polarization converters [5], scintillators [6], optical sensors [7], integrated couplers/splitters [8] and optical isolators [9]). As such, the photonic device market is projected to grow from the current multimillion dollar-per-year industry into one valued at several billion dollars per year by 2010 [10]. Overcoming the current technological barrier of materials processing costs, vis à vis those for electronics [1] would represent an additional major advantage for photonic devices. Such devices have largely been based on oxide crystals (e.g., $LiNbO_3$ and $LiTaO_3$) and III–V semiconductors (e.g., GaAs and $Al_xGa_{1-x}As$). In both cases, advantages gained by an application-specific material property have not sufficiently out-weighed device costs. The manifestation of this, often combined with difficulties in crystal growth and integration, has inspired investigators to continue to search for more suitable materials [12].

* Corresponding author. Tel.: +1-908 445 4946; fax: +1-908 445 6264; e-mail: riman@rci.rutgers.edu.

[1] It is interesting to note that in the case of optical fibers for local area networks (LANS), the cost per drop for fiber now is less than the cost per drop for coaxial cable. See Ref. [11].

This paper conceptually and experimentally explores the potential of fluoride glasses for use in the field of planar integrated photonics. We begin by comparing the properties of fluorides with materials currently utilized for such applications and show the fluorides to be attractive alternatives in terms of meeting the challenge of cost competitiveness and retaining the requisite properties. The current status of thin-film fluoride materials (amorphous and crystalline) is discussed with particular attention paid to the viable role sol–gel processing would play in planar device synthesis. We conclude by suggesting some novel directions and classes of planar devices that benefit from both the unique properties of fluoride glasses and those imparted by sol–gel approaches.

2. Photonic material considerations and comparisons

Several properties of interest for planar integrated optic devices are compared in Table 1 for fluoride and silica glasses, gallium arsenide, and lithium niobate. The latter three materials have received the most attention for photonic applications, yet fluorides possess some attractive features that warrant further consideration. Several such aspects deserving special recognition are illustrated.

2.1. Index of refraction

Lithium niobate [13], as well as compositions in the gallium arsenide/aluminum arsenide family, have large indices of refraction [14]. In contrast, fluoride materials are well known for their relatively low indices and optical dispersions [15]. Devices integrated with materials whose indices are much greater than the silica fibers invariably providing the optical input, incur large power losses due to Fresnel reflections at an interface. A gallium arsenide/silica interface produces a 17% reflection per surface, whereas a fluoride/silica boundary provides a 0.04% reflective loss per surface. These losses are technologically significant since power lost by reflection subsequently must be overcome by signal amplification. Utilization of fluoride films would minimize the requisite degree of amplification with respect to the III–V semiconductors or oxide crystals.

2.2. Attenuation and luminescence

The weak bonding and greater reduced mass of the fluorine-cation complex, with respect to the silicon–oxygen system, leads to decreased intrinsic phonon scattering, and an infrared transmittance to longer wavelengths [16]. Theoretically, this reduced scattering and infrared transmittance results in a hundred-fold increase in maximum transparency with respect to silicate glasses. Although fluoride glasses have yet to exhibit losses approaching the theoretical limit ($\sim 10^{-3}$ dB/km, or 0.023% power loss in 1 km), current attenuations remain orders-of-magnitude below the oxide crystals and III–V semiconductors [17]. We note that the need to achieve near-theoretical transparency is far less crucial in integrated photonic systems, than in long-haul cables, since typical planar waveguide path-lengths are on the order of centimeters.

The reduced phonon energy, brought about by the weaker bonding and greater reduced mass in fluoride systems, also provides active dopants with longer excited-state lifetimes and, consequently, luminescence at wavelengths not attainable from most other hosts, including the silicates. For this reason, fluoride glasses are receiving a great deal of attention for 1.3 μm optical amplifiers, highly efficient solid state lasers and upconversion sources [3]. In comparison, lithium niobate may also be doped to achieve radiative emissions, however its structure imparts a biaxial optical indicatrix which causes sharp and polarized absorption and fluorescence features from the active species [17]. Gallium arsenide is a direct bandgap semiconductor which may be electrically-excited into the generation of light [18]. Emissions are tunable over the fiber optic telecommunications windows by aluminum arsenide and indium phosphide modifications to the nominal composition [19]. Extended clarity into the infrared generally is coupled with an electronic edge shift towards the visible which could pose a disadvantage if considerable absorption occurs at a pump wavelength. This is rarely an issue in excitations of dopants in fluoride hosts, but may be problematic in chalcogenide glasses or integrated gallium arsenide components.

Table 1
Comparison of selected properties of interest for integrated photonic applications

Property	v-SiO_2	GaAs	$LiNbO_3$	Fluoride	Desired value
Refractive index, n	1.458	3.5	2.2	1.52	match SiO_2
Fresnel reflection (%) (w.r.t. SiO_2)	0	17	4	0.04	small
Attenuation (dB/km)	0.16 @ 1.55 μm	1–2 (dB/m) @ 1.3 μm	0.5 (dB/m) @ 1.3 μm	10^{-3} (theory) @ 3.44 μm	low @ telecom window
Transmission (μm)	0.2 → 4	0.9 → 12	0.2 → 5	0.3 → 6	visible → IR
Emission (1.3 μm)	Nd (poor)	elec. induced	Nd (poor)	Pr (good)	good
(1.5 μm)	Er (standard)	elec. induced	Er	Er	Er
Density ($*10^3$ kg/m^3)	2.2	5.32	4.64	4.61	
Atomic structure	isotropic glass	cubic crystal ($\bar{4}$ 3 m)	trigonal crystal (m)	isotropic glass	depends on application
Thermal stability range (°C)	T_g = 1100 T_x = 1575 T_m = 1700	T_m = 1238	T_m = 1253	T_g = 250 T_x = 340 T_m = 490 (ZBLAN)	depends on application (arctics ⇔ tropics)
Thermal expansion ($\times 10^{-7}$/K)	5.5	60	α_{33} = 75 α_{11} = α_{22} = 154	150–180	match substrate
Chemical stability 20	stable OH, unstable HF	20 μm/min (1 HF:3 HNO_3)	tenths of Å/min (HF:HNO_3)	unstable OH stable HF	depends on application
Poisson's ratio	0.16	0.312	ν_{21} = 0.197, ν_{31} = 0.249	0.3	
Thin film technology [a]	· CVD · sputtering · sol–gel · IE	· EG · VPE · MOCVD · MBE	· LPE · EG · IE · II	· sol–gel · evaporation · IE · MBE	· reliable · reproducible
Cost (thin film)	low	high	high	low (sol–gel)	low

[a] Thin film technology abbreviations: ion exchange (IE), epitaxial growth (EG), vapor phase epitaxy (VPE), metal organic chemical vapor deposition (MOCVD), molecular beam epitaxy (MBE), and ion implantation (II).

2.3. Planar waveguide criteria

The waveguide structures of photonic circuits often are asymmetric, i.e., the two materials cladding the light-guiding core are of differing refractive indices. This inequality in clad index allows for a condition in which an absolute cut-off exists for propagation modes [20]. This cut-off condition for asymmetric planar guides restricts the core thickness, D, to

$$D \geq \frac{\lambda}{4}\frac{1}{\mathrm{NA}},$$

where λ is the wavelength of the light to be transmitted and NA is the numerical aperture of the structure. Computations performed for the materials compared in this work are shown in Table 2. The inverse proportionality of the critical film thickness with numerical aperture implies that the greater the difference in refractive index between core and clad (i.e., the higher the degree of optical confinement), the thinner the requisite film. Thus, when selecting a waveguiding system, the issue of film thickness may lead to physical (and economical) constraints that cannot be overcome by processing techniques. For instance, growth of a 4 μm $LiNbO_3$ film by MBE is a formidable task while deposition of a 0.7 μm fluoride film by sol–gel methods may be routinely achieved.

2.4. Acousto–optic (AO) properties

Transparent materials act as optical phase gratings when a sound wave passes through them. This photoelastic effect, unlike the linear electro–optic effect, is present in all materials, therefore the *a priori* spectrum of transparent materials is unlimited [21]. Devices based on this phenomenon include optical filters tunable over a much broader frequency range than electro–optic systems, optical deflectors for laser scanners, and optical modulators which require lower drive powers, simpler electronics, and have higher safety factors than their electro–optic counterparts [22]. Despite a great deal of materials research into the improvement of these devices, the AO properties of fluoride glasses have received only limited attention to-date, with most work quantifying photoelastic coefficients [23]. We now illustrate the impact of materials selection on the important device-related parameters of AO Figure of Merit, acoustic impedance, and acoustic attenuation.

The most commonly compared figure of merit is M_2 which is a proportionality between the applied acoustic wave intensity and corresponding modification to the refractive index. The figure of merit is given by [21]

$$M_2 = \frac{n^6 p^2}{\rho v^3},$$

where n is the refractive index, p is the appropriate photoelastic coefficient (Pockels' coefficient), ρ is the mass-density, and v is the acoustic velocity (in the direction pertinent to p). By virtue of their low acoustic wave velocities and relatively high densities, fluoride glasses exhibit acousto–optic figures of merit as much as 40% that of $LiNbO_3$, and twice that of silica, which, to-date, is the most successful material used in optical switches, despite its small magnitude [12]. The efficacy of the coupling between the propagating acoustic modes in the AO material and the surrounding media is related to the acoustic impedance (Z_{ac}). This occurs in a manner analogous to the way the Fresnel reflection of an electromagnetic (EM) wave at an interface is mediated by the EM impedances. The acoustic impedance is the product of mass density and acoustic wave velocity [24]. Therefore, fluorides possess acoustic impedances which may make them well-suited as matching materials in low Z_{ac}, applications.

In addition to the moderate FOM and low acoustic impedance, we find the acoustic attenuation to be, perhaps, the acoustic property by which devices

Table 2
Critical film thickness as a function of typical numerical apertures for various asymmetric slab waveguide structures at two telecommunication windows

System	NA	D (μm)	
		1.3 μm	1.5 μm
GaAs/AlGaAs	0.1	3.25	3.75
$LiNbO_3$ /Ti:$LiNbO_3$	0.2	1.62	1.87
ZBLA on CaF_2	0.44	0.74	0.85
ZBLA on LiF	0.56	0.58	0.67
ZBLA on MgF_2	0.58	0.56	0.64

utilizing fluoride materials gain the most benefit [25]. The acoustic attenuation, α_L, measures the spatial power-loss rate of an acoustic wave travelling through a solid. For a longitudinal plane wave propagating through a material, α_L may be calculated from the Woodruff–Ehrenreich equation [26],

$$\alpha_L = \frac{\gamma^2 \kappa T}{\rho v_L^5}(\omega^2),$$

where, γ is the Grüneisen constant, κ is the thermal conductivity, T is the absolute temperature, ρ is the mass-density, v_L is longitudinal wave velocity, and ω is the angular frequency of the acoustic wave. The theoretical acoustic attenuation (dB/cm) at 1 GHz is calculated to be $\alpha_L = 0.6$ dB/cm. This value is only slightly larger than the 0.2 dB/cm theoretical Akheiser attenuation for sapphire [28]. Table 3 quantifies the M_2 FOMs, acoustic impedances, and acoustic attenuations for the optical materials contrasted in this work. We find the fluorides (in both bulk and thin-film form) to possess unique properties which should mark them as materials to receive attention for acousto–optic applications.

2.5. Thermal stability

Fluorides have low thermal stability, which means a lower melting, crystallization, and glass transition temperatures than observed with silicate glass formers [16]. Calorimetric studies [31] indicate fluoride glasses form from highly-coordinated cation-fluorine anion species based on the 'confusion' principle rather than the sluggishness of the polymeric network as in silicate hosts. Sol–gel methods may produce nanostructured materials that rapidly densify at temperatures which are considerably less than T_g (ca. 200°C) [32]. This advantage is among the most important for thermally unstable fluoride glass systems. Unlike materials processed by melt-quench techniques, viscous-sintering promotes stability and compositional flexibility since the glass never experiences the crystallization temperature, T_x. Further, such low synthesis temperatures facilitate coprocessing of fluoride glasses with plastics (e.g., polyimide) [33], which are finding increased use in electronic devices and conformable coatings. These low fabrication temperatures are also advantageous when thermal expansion mismatches exist. Substrates based on the GaAs–AlAs family have thermal expansion coefficients [14] roughly one-half that of the typical fluoride glass. In these cases, the low glass transition temperatures of the fluorides facilitate the relaxation of stresses induced by the expansion mismatch. In addition, with a stress-free film at T_g, upon cooling, the higher expansion coefficient ensures a state of compression in the film, which imparts mechanical stability. In the case of integration with $LiNbO_3$, thermal expansion coefficients of approximately 154 $\times 10^{-7}$/K ($\alpha_{11} = \alpha_{22}$) [13] are well-matched to that of the fluorides ($\sim 160 \times 10^{-7}$/K) [15] which minimize stresses in the deposited films.

2.6. Fabrication methodologies

Table 4 compares the advantages and disadvantages of the various techniques [34] associated with the fabrication of gallium arsenide, lithium niobate, silica and fluoride glass films. Gallium arsenide profits from a well-developed epitaxy, doping, masking, and etching techniques. The solid solution formed as

Table 3
Comparison of acousto–optic figure of merit, acoustic impedance, and acoustic attenuation for gallium arsenide, lithium niobate, and silica and fluoride glasses

Material	Acoustic velocity (m/s)	Pockels' coefficient	M_2 FOM ($\times 10^{-15}$ s^3/kg)	Acoustic impedance (10^6 kg/s m^2)	Acoustic attenuation (dB/cm at 1 GHz)
v-SiO_2	5950	0.270 [30]	1.51	13.1	12.1 [28]
GaAs	5150	0.203 [30]	104.2	27.4	2.7 [28]
$LiNbO_3$	6570	0.284 [30]	6.95	30.5	0.1 [29]
ZBLA	3952 [15]	0.251 [24]	2.74	18.2	0.6 [a]

[a] The appropriate physical constants for a ZBLA glass [15,27] are ($T = 300$ K): $\gamma = 2.6$, $\kappa = 0.4$ W/m · K, $\rho = 4610$ kg/m^3, $v_L = 3952$ m/s.

Al is substituted for Ga is well characterized, provides good lattice matching, and allows for index modification to achieve a waveguide geometry [14]. However, fabrication methods offer very slow growth rates (10–30 nm/h) [34] and, often, with hazardous precursors. Lithium niobate waveguides are typically fabricated either by lone Ti diffusion, or codiffusion of Ti and H for Li. These techniques also are well

Table 4
Comparison of techniques for planar waveguide production

Deposition / growth process	Methodology	Advantages	Disadvantages
Vacuum deposition including: Resistive heating and E-beam	Heat material to T_m. Evaporate to adhere on substrate.	Simple. Good for metals (e.g., Ag, Au, and Al).	Some metals too refractory (e.g., Ti) or reactive. Line-of-sight, and high vacuum
RF sputtering	Substrate (anode) close to target Ar^+ plasma sputters atoms from target to substrate.	Conformal coating on metals and dielectrics. Can coat nonplanar substrates. Inert argon atoms produce no added reactions.	More complicated apparatus. Long time to deposit thick layers since sputtering may be slow (~ 0.01 μm/min for glassy materials).
Chemical vapor deposition (CVD) including: PECVD (lowest temp. via plasma assisted deposition), LPCVD (low pressure), and MOCVD (metal-organic precursors).	Hot gas mixture passed over substrate so film of correct composition gradually deposited following reaction near surface.	Very versatile, can produce refractive index changes for planar silica waveguides by altering gas flow rates thus changing composition.	Difficult to ensure uniformity (thickness and stoichiometry) since temp., comp., concentration, and gas velocity can vary along length. Precursor gases are hazardous.
Epitaxial growth including: LPE (liquid phase), VPE (vapor phase), and MBE (molecular beam).	Use substrate atomic lattice as template for crystal lattice of film. Homoepitaxy: Substrate and layer same. Heteroepitaxy: Different materials.	$Al_xGa_{(1-x)}As$ on GaAs good since lattice parameters almost independent of x. VPE very good. MBE low temp., virtually no diffusion.	LPE difficult to maintain composition. High temp., diffusion smoothens interface. VPE hazardous precursors. MBE slow growth rates: 0.1–1 μm/h (0.1 nominal).
Diffusion, including: in- and out-diffusion	Substrate in contact with dopant. Elevated temp., dopant migrates into lattice.	Well-developed for Ti metal into $LiNbO_3$. Circular cross-sections with Gaussian profile allows good coupling to optical fibers.	Generally long times at elevated temp. Crystal orientation strongly influences properties in diffused region.
Ion exchange	Substrate in liquid. Two species codiffuse.	Lower temp. than diffusion. Electric field increases rate, provides uniform, deep profiles.	Only relatively small changes in properties ($\Delta n \sim 0.1$). Low temp. since thermally anneal-out profile.
Proton exchange	Replace Li^+ with H^+ from benzoic acid melt (mainly for $LiNbO_3$).	Near-step index geometry.	Crystal structure inhibits isotropy, hence polarization sensitive.
Ion implantation	Ions extracted electrostatically from melt, collimated into a beam.	Ion distribution well controllable and defined.	High vacuum, expensive equipment. Thermal annealing necessary.
Sol–gel	Solution-based method to 3D network by molecular polymerization or agglomeration of colloidal particles.	Wide range of materials. Planar geometries more compatible with surface modification techniques. High purity and homogeneity.	Production of non-oxide materials not well established. In case where existing, reactive gases generally hazardous.

developed and may provide for complicated structures [35]. However, the crystal anisotropy strongly influences the optical and electronic properties of the diffused region, and only relatively small changes in index are achievable [36]. This, as well as difficulties in growth on, and integration with semiconductor materials, propels the cost to almost prohibitive levels [12].

Preliminary efforts have been conducted into thin-film fluorides via electron-beam depositions [37], vapor depositions [38], PECVD [39], and evaporation techniques [40], all with limited success. The multicomponent nature of fluorides causes difficulty with vapor-transport methodologies owing to vapor-pressure differences between constituents. More recently, higher quality amorphous fluoride thin films have been prepared by further efforts in thermal evaporation [41] as well as novel attempts with physical vapor deposition (PVD) [42] and ion exchange [43] techniques. The ZrF_4 films [41] were hygroscopic and contained both reduced zirconium species and oxide contaminants. The latter most likely negates any dopant luminescence indicative of a low-phonon energy host until oxygen impurity concentrations are minimized. Fluorescent emissions characteristic of Er^{3+} doped fluoride glasses, including upconversion, were exhibited by the PVD films [42]. However, the requirement of constituents with similar vapor pressures severely limits the compositional range. The concept of ion exchange between a bulk glass and molten salt has received much attention, albeit mostly for silicate glasses [44]. In the fluoride system, earlier studies with chlorine–fluorine exchange [45], as well as the more recent observation of waveguiding in ZBLAN and BIG glasses [43] via Li^+ or K^+ for Na^+ exchange demonstrate feasibility. Single-crystal films of ZnF_2 and LaF_3/SrF_2 have been synthesized via MBE [46,47]. The earlier work [46] considers the observation of erbium upconversion in channel waveguides which where fabricated by ion milling. The later MBE work [47] discusses promising results on undoped LaF_3. Propagation losses of 3.7 dB/cm were measured at 633 nm. However, films thicker than approximately 1 μm exhibited cracking.

Our work on sol–gel approaches [32,33,48] provides another powerful method for thin film deposition. Advantages include high purity (i.e., precursors which are easily purified), amenability to forming many shapes (e.g., films, coatings, powders, fibers, monoliths, gels), atomic-scale mixing, large compositional flexibility, and low-temperature viscous-sintering. Synthesis is a multistep process involving a sol–gel reaction and a reactive atmosphere treatment. The first step is the synthesis of a hydrous oxide containing the requisite cations; this is achieved by hydrolyzing and condensing the precursor solution. The second step is a low-temperature reactive atmosphere treatment using anhydrous hydrogen fluoride gas to convert the hydrous oxide to a fluoride. Subsequent thermal processing at the glass transition temperature viscous-sinters the film [49].

3. Current status of sol–gel-derived fluorides

X-ray-amorphous and crack-free ZBLA ($57ZrF_4 \cdot 36BaF_2 \cdot 4LaF_3 \cdot 3AlF_3$, in mol%) fluoride thin films have been deposited on calcium fluoride, polyimide, silicon, gallium arsenide, lithium niobate, and sapphire substrates [33]. Our more recent studies considered the optical waveguiding of ZBLA films on single-crystal calcium fluoride substrates. A 25 μm fluoride film was sandwiched between the substrate and a second CaF_2 blank following fluorination at 200°C for 1 h. Waveguiding through the 25 mm path-length was observed following white-light illumination with a transmitted-light microscope. This represents the first observed confined propagation in a sol–gel-derived planar fluoride structure. Geometric pattering of similar films was accomplished by a novel rapid prototyping method [50] which facilitates the development of unique waveguide structures that can be designed on a computer terminal and produced within hours of its conception.

The spectroscopic properties of ZBLA films, derived from metal-organic precursors, was discussed in our earlier work [33]. Characteristically low-phonon energy emissions from erbium were not observed due to phonon quenching. Remnant carbonaceous species from the metal-organic precursors were proposed as the cause of this problem following the results of other studies on the optical and electrical properties of these materials [32,51]. The inability to generate characteristic luminescence relegates these materials only to passive applications. Melting of

these sol–gel fluoride materials [52] does produce characteristic emissions, however, the ability to fabricate thin-films is lost. Sol–gel-derived fluorides for active applications may be synthesized from metal-inorganic precursors. Characteristically low-phonon energy emissions from these materials was first discussed by Dejneka [51] investigating the properties of Eu^{3+}: ZrF_4 powders derived from an aqueous zirconium hydroxychloride solution. More recently, we showed metal-inorganically-derived Er^{3+}: ZrF_4 powders and films [53] to exhibit intrinsic luminescence.

4. Future directions and potential applications of sol–gel-derived fluorides

We now consider novel planar photonic applications of fluorides based on their unique material properties as well as those imparted by the benefits of a sol–gel synthesis approach. Several possibilities are discussed below.

4.1. The planar fluoride acousto–optic (AO) modulator

Modulators are photonic components which are used to encode information onto an optical beam. High speed systems utilize [12] the electro–optic effect in some materials for this purpose, yet the acousto–optic effect is desirable in lower bit-rate applications since it requires lower drive powers and simpler electronics, and has higher safety margins [22,29]. We have shown the fluorides to possess AO figures of merit making them worth considering for AO modulators especially in light of the low-cost and ease of the sol–gel process.

One possible configuration utilizes the ability of sol–gel to deposit films on a variety of piezoelectric substrates. The integration of these materials is necessary, since a piezoelectric substrate acts as a transducer to generate the acoustic waves used to produce the refractive index grating. The substrate selection is based on two main criteria. First, the substrate must be stable against a fluorinating atmosphere. Secondly, consideration must be given to the thermal expansion differences between the substrate and the thin-film fluoride. In both cases, $LiNbO_3$ and PVDF (poly(vinylidene) difluoride) satisfy these conditions. PVDF is insensitive to the HF atmospheres used to process the sol–gel fluorides. Furthermore, its polymeric nature lends pliability to a system integrated with it. Lithium niobate is strongly piezoelectric ($k^2 \simeq 40\%$) [54], stable in HF acid (etch rate is ~ 0.01 nm/min) [55] and its coefficient of thermal expansion matches the fluorides. Layers of a lower-index fluoride material may be deposited to act as a cladding, The low temperature synthesis of an fluoride AO modulator allows for coprocessing with a variety of substrate materials. This leads to greater ease in fabrication and lower costs.

4.2. The planar fluoride Q-switched laser

The acousto–optic effect in fluorides further gains utility in Q-switched laser schemes. In these devices, the presence of an acoustic wave spoils the optical resonance of the laser cavity. The excitation energy used to pump the active ion is stored in a larger-than-normal population inversion. Subsequent removal of the acoustic disturbance at the peak inversion value reinstates the resonance and produces a rapid and high intensity pulse [56]. This effect generally is too slow for signal modulation in most telecommunication systems, however, it does find utility in high-energy pulse generation for lidar, laser range-finding, cutting/welding, and some military applications.

Materials which possess large acousto–optic figures of merit are desirable as they can diffract an optical beam more efficiently with lower acoustic wave intensities than permissible with lower FOM materials. We believe the utilization of planar fluoride materials is of interest from this regard as well as from the point of low acoustic attenuation. In addition, the fluorides not only enable efficient switching of the laser, they also enable a greater number of laser emissions.

4.3. The planar evanescent field coupler / splitter

The fabrication of planar waveguides also enables the creation of novel optical couplers and splitters. Applications based on this technology include signal multiplexers and demultiplexers which are efficient methods for increasing bandwidth in telecommunica-

tion networks [57]. Two prefluorinated strip guides positioned face-to-face, with an intermediate sol–gel buffer layer, may be used to couple light from one core to the other. Waveguiding regions may be doped with materials to raise the refractive index, whereas the buffer regions would contain additions which lower the index. The small film thicknesses achievable with sol–gel techniques would enhance the coupling efficiency and permit shorter device lengths. Planar fluoride splitters may also benefit from its low phonon energy. Zero-loss splitters can be fabricated by suitable doping of the waveguide so that signal gain is used to overcome splitting and propagation losses.

4.4. The planar remote infrared chemical sensors

The chemical inertness of fluorides to many types of highly corrosive environments (e.g., HF, HCl, ...) allows for the sensing of many species which would not be possible with oxide hosts. In addition, spectroscopy may be performed on materials exhibiting absorptions further into the infrared than accessible with silica-based optics (e.g., CO at 4.6 μm, CO_2 at 4.2 μm, HF at 1.25 μm, HCl at 3.5 μm, formaldehyde at 3.3 μm [58], ...). Waveguide losses may be monitored over a spectrally broad range to observe those energies absorbed in exciting vibrational modes in the particular molecule under investigation. Correlation between absorption intensity and sensate concentration allows quantitative analysis. Liquids and gaseous species may be examined.

4.5. The planar electro–optic modulator

The vitreous nature of fluoride glasses precludes the existence of linear electro–optic properties. However, the porous nature of sol–gel-derived materials is well-suited for the incorporation of specific species into the network. Nano-sized powders with active features (e.g., electro–optic $LiNbO_3$) may be colloidally suspended into the sol, or doped into the open structure post gelation. In addition, the planar geometry of the strip waveguide is ideal for subsequent pattering of an external conductor since the low fabrication temperature facilitates coprocessing. Modulation in the electric field produced between conducting clad layers and the substrate will control light propagation paths and permit signal manipulation. This composite material potentially allows for the beneficial properties of the active dopant in a fluoride matrix. New electro–optic modulators and filters, both having great technological importance, may be produced at low temperatures and at a greatly reduced processing cost.

5. Conclusions

We have shown by comparison to existing photonic materials that fluorides warrant consideration for use in integrated optic applications. Moderate acousto–optic figures of merit, coupled with low acoustic impedances and attenuations mark the fluorides as materials to receive attention for acoustic applications. Such AO devices may represent the greatest prospect for the commercialization of sol–gel fluoride materials. The ability to make waveguiding, and patternable fluoride films via sol–gel further enhances the advantages gained by their use, based on the simplicity and low-cost of the synthesis. For passive applications, metal-organic precursors would provide viable property attainment, whereas for active devices, inorganic precursors need to be used. In addition to the material properties of the sol–gel-derived fluorides, we have discussed novel ways in which to integrate them into planar photonic devices. The future remains bright for the utilization of fluoride optical materials in telecommunications. Considerable potential also exists in previously unconsidered directions, especially those related to integrated photonics.

Acknowledgements

The authors wish to acknowledge Professor Stephen Danforth, and Dr. Remco van Weeren and Dr. Mukesh Agarwala of Rutgers University for their collaboration on the guide pattering via rapid prototyping. Further thanks are extended to Joel Plewa for some of the film and powder synthesis and characterization. This work was supported by the Rutgers University Fiber Optic Materials Research Program, The Center for Ceramic Research, and the New Jersey Commission on Science and Technology.

References

[1] K. Hagimoto, S. Nishi, K. Nakagawa, IEEE J. Lightwave Technol. 8 (1990) 1387–1395.

[2] T.V. Higgins, Laser Focus World (Nov. 1995) 93.

[3] M.J.F. Digonnet, ed., Rare Earth Doped Fiber Lasers and Amplifiers (Marcel Dekker, New York, 1993); A. Bjarklev, Optical Fiber Amplifiers, Design and System Applications (Artech House, Boston, 1993).

[4] D.W. Hewak, R.S. Deol, J. Wang, G. Wylangowski, J.A. Mederios Neto, B.N. Samson, R.I. Laming, W.S. Brocklesby, D.N. Payne, A. Jha, M. Poulain, S. Otero, S. Surinach, M.D. Baro, Electron. Lett. 29 (1993) 237.

[5] K. Mertens, B. Scholl, H.J. Schmitt, IEEE J. Lightwave Technol. 13 (1995) 2087.

[6] M. Poulain, J. Non-Cryst. Solids 184 (1995) 103.

[7] C. Piraud, E.K. Mwarania, J. Yao, K. O'Dwyer, D.J. Schiffrin, J.S. Wilkinson, IEEE J. Lightwave Technol. 10 (1992) 693.

[8] J.L. Jackel, W.J. Tomilson, Opt. Photon. News 6 (1995) 47.

[9] T. Shintaku, Appl. Phys. Lett. 66 (1995) 2789.

[10] M.S. Goodman, E. Arthurs, in: Integrated Optoelectronics, ed. M. Dagenais, R.F. Leheny and J. Crow (Academic Press, New York, 1995) p. 3.

[11] G. Kotelly, Lightwave (Dec. 1994) 6.

[12] R.F. Service, Science 267 (1995) 1918.

[13] R.S. Weis, T.K. Gaylord, Appl. Phys. A37 (1985) 191.

[14] S. Adachi, J. Appl. Phys. 58 (1985) R1.

[15] D. Tran, G.H. Sigel Jr., B. Bendow, IEEE J. Lightwave Technol. 2 (1984) 566.

[16] R. Gatzke, Ceram. Bull. 68 (1989) 1946.

[17] E. Lallier, Appl. Opt. 31 (1992) 5276.

[18] S.L. Chuang, Physics of Optoelectronic Devices (Wiley, New York, 1995) pp. 707–711.

[19] J.E. Bowers, M.A. Pollack, in: Optical Fiber Telecommunications II, ed. S.E. Miller and I.P. Kaminow (Academic Press, New York, 1988) p. 509.

[20] D. Marcuse, Theory of Dielectric Optical Waveguides (Academic Press, New York, 1991) pp. 1–49.

[21] D.A. Pinnow, IEEE J. Quantum Electronics 6 (1970) 223.

[22] P.K. Das, C.M. DeCusatis, Acousto–Optic Signal Processing: Fundamentals and Applications (Artech House, Boston, MA, 1991) p. 171.

[23] J. Schroeder, G.A. Floudas, M.A. Stiller, M.G. Drexhage, in: Materials Science Forum, Vol. 6 (TransTech, Aedermannsdorf, 1985) p. 577.

[24] A.P. Goutzoulis, W.R. Beaudet, in: Design and Fabrication of Acousto–Optic Devices, ed. A.P. Goutzoulis and D.R. Pape (Marcel Dekker, New York, 1994) p. 285.

[25] J. Ballato, A. Ballato, R.E. Riman, 'A phenomenological approach to the calculation of acoustic attenuation in crystals and glasses', manuscript in progress.

[26] T.O. Woodruff, H. Ehrenreich, Phys. Rev. 123 (1961) 1553.

[27] W.J. Tropf, M.E. Thomas, T.J. Harris, in: Handbook of Optics, Vol. II: Devices, Measurements, and Properties, ed. M. Bass (McGraw-Hill, New York, 1995) pp. 33.2.

[28] C.F. Quate, A. Atalar, H.K. Wickramasinghe, in: Acoustic Microscopy with Mechanical Scanning – A Review, ed. B.T. Khuri-Yakub and C.F. Quate, (SPIE Optical Engineering, Bellingham, WA, 1992) p. 37.

[29] J. Xu, R. Stroud, Acousto–Optic Devices: Principles, Design, and Applications (Wiley, New York, 1992) p. 619.

[30] I.C. Chang, in: Handbook of Optics, Vol. II., Devices, Measurements, and Properties, ed. M. Bass (McGraw-Hill, New York, 1995) pp. 12.1.

[31] I-C. Lin, A. Navrotsky, J. Ballato, R.E. Riman, 'A calorimetric study of fluorozirconate melts, glasses, and crystals: Thermodynamic aspects of glass formation in fluorozirconates', submitted to J. Non-Cryst. Solids.

[32] M. Dejneka, PhD thesis, Rutgers University (1995).

[33] J. Ballato, M. Dejneka, E. Snitzer, R.E. Riman, W. Zhou, J. Mater. Res. 11 (1996) 841.

[34] R. Syms, J. Cozens, Optical Guided Waves and Devices (McGraw-Hill, New York, 1992) ch. 13, pp. 390–427.

[35] M. McWright Howerton, W.K. Bums, P.R. Skeath, A.S. Greenblatt, IEEE J. Quantum Electronics 27 (1991) 593.

[36] W. Sohler, Thin Solid Films 175 (1989) 191.

[37] A.J. Bruce, G. Zydzik, M. Chui-Sabourin, in: Materials Science Forum, Vols. 67&68 (TransTech, Aedermannsdorf, 1991) p. 377.

[38] C. Jacoboni, B. Boulard, P. Baniel, H. Poignant, in: Materials Science Forum, Vols. 19&20 (TransTech, Aedermannsdorf, 1987) p. 253.

[39] K. Fujiura, Y. Nishida, H. Sato, S. Sugawara, K. Kobayashi, Y. Terunuma, S. Takahashi, J. Non-Cryst. Solids 161 (1993) 14.

[40] H. Poignant, J. LeMellot, Y. Bossis, in: Materials Science Forum, Vol. 5 (TransTech, Aedermannsdorf, 1985) p. 79.

[41] R.M. Almeida, P.J. Morais, J. Non-Cryst. Solids 184 (1995) 93.

[42] M.F. Joubert, A. Remillieux, B. Jacquier, J. Mugnier, B. Boulard, O. Perrot, C. Jacoboni, J. Non-Cryst. Solids 184 (1995) 341.

[43] C. Charron, E. Fogret, G. Fonteneau, R. Rimet, J. Lucas, J. Non-Cryst. Solids 184 (1995) 222.

[44] R.V. Ramaswany, R. Srivastava, IEEE J. Lightwave Technol. 6 (1988) 984.

[45] S. Ko, R. Doremus, X.S. Guo, W. Landford, J. Mater. Res. 5 (1990) 202.

[46] M. Lui, R.A. McFarlane, D. Yap, D. Lederman, Electron. Lett. 29 (1993) 172.

[47] D.K. Fork, F. Armani-Leplingard, M. Lui, R.A. McFarlane, IEEE J. Lightwave Technol. 14 (1996) 611.

[48] R.E. Riman, M. Dejneka, J. Ballato, E. Snitzer, Eur. J. Solid State Inorg. Chem. 32 (1995) 873.

[49] A.M. Mailhot, A. Elyamani, R.E. Riman, J. Mater. Res. 7 (1992) 1534.

[50] J. Ballato, M. Agarwala, R. van Weeren, R.E. Riman, S.C. Danforth, Electron. Lett. 33 (1997) 83.

[51] M. Dejneka, E. Snitzer, R.E. Riman, J. Non-Cryst. Solids 202 (1996) 23.

[52] M. Dejneka, R.E. Riman, E. Snitzer, J. Am. Ceram. Soc. 76 (1993) 3147.

[53] J. Ballato, 'Sol–gel synthesis of rare-earth-doped halide optical materials for photonic applications', PhD thesis, Rutgers University, in progress.
[54] A. Ballato, Y. Cho, L. Kovacs, R.S. Weis, K. Yamanouchi, K. Polgar, in: Properties of Lithium Niobate (INSPEC, The Institution of Electrical Engineers, London, 1989) p. 109.
[55] C.W. Pitt, in: Properties of Lithium Niobate (INSPEC, The Institution of Electrical Engineers, London, 1989) p. 227.
[56] J. Hawkes, I. Latimer, Lasers, Theory and Practice (Prentice Hall, New York, 1995) p. 437.
[57] R. Syms, J. Cozens, Optical Guided Waves and Devices (McGraw-Hill, New York, 1992) ch. 13, p. 442.
[58] G. Mazé, V. Cardin, F. Chiquet, M. Poulain, in: Optical Fiber Sensors, Springer Proceedings in Physics, Vol. 44, ed. H.J. Arditty, J.P. Dakin and R.T. Kerset (Springer, Berlin, 1989) p. 20.

Sol-gel synthesis of rare-earth-doped lanthanum halides for highly efficient 1.3-μm optical amplification

John Ballato, Richard E. Riman, and Elias Snitzer

Fiber Optic Materials Research Program, Department of Ceramic Science and Engineering, Rutgers, The State University of New Jersey, Brett and Bowser Roads, Piscataway, New Jersey 08855-0909

Received January 22, 1997

Praseodymium- and dysprosium-doped lanthanum halide powders have been synthesized by a sol-gel–reactive-atmosphere approach. Emission at 1.3 μm from a sol-gel-derived material was observed for the first time to our knowledge. Measured lifetimes corresponded to radiative quantum efficiencies of approximately 8% for Pr^{3+}:LaF_3, 72% for Pr^{3+}:$LaCl_3$, and 78% for Dy^{3+}:$LaCl_3$. The spectroscopic properties of these hosts are shown to be comparable with those of melt-grown single-crystal analogs, verifying the ability of inexpensive and low-temperature solution-based methodologies to produce low-phonon-energy materials. © 1997 Optical Society of America

There has been great growth in photonic materials and device research as a result of both the rapid growth of the telecommunications industry and the expected traffic requirements for interactive video and multimedia services. These trends are incentives to study novel ways of expanding the information-carrying capacities of the existing optical fiber infrastructure because it is far more economical to increase bandwidth than to install new fiber.[1] Economic aspects of all-optical transmission systems were not nearly so favorable until the erbium-doped fiber amplifier became a practical device to provide efficient, low-noise broadband gain for the 1.55-μm minimum-loss window.[2] The result is a global optical-amplifier market expected to be worth nearly $1.2 billion/year by 2004.[3] However, erbium-doped fiber amplifiers are not appropriate for operation at the 1.3-μm zero-dispersion window that dominates existing fiber communications. For these reasons there is an international search for host materials suitable for 1.3-μm optical amplification.

These optical amplifiers use Pr^{3+} or Dy^{3+} dopants to luminesce and provide gain at 1.3 μm. Praseodymium[4] (Pr^{3+}) has been more widely studied and has reached some level of commercialization[5] despite the low quantum yield from current hosts. Dysprosium[6] (Dy^{3+}) more recently has attracted interest because its absorption cross section is significantly larger than that of Pr^{3+} and would greatly lessen the requisite amplifier length. However, questions remain as to the influence of excited-state absorption on the 1.3-μm emission. Radiative transitions between rare-earth excited states are more efficient when host phonon energies are minimized. Toward this end, we considered the synthesis of doped lathanum halides. Material advantages with respect to silicate and chalcogenide hosts are reduced phonon energies (e.g., $\hbar\omega_{SiO_2} = 1100\ cm^{-1}$, $\hbar\omega_{As_2S_3} = 350\ cm^{-1}$, $\hbar\omega_{LaF_3} = 350\ cm^{-1}$, and $\hbar\omega_{LaCl_3} = 260\ cm^{-1}$) and very high solubilities for rare-earth dopants. The latter advantage allows for large sensitizing concentrations while an optimum luminescent dopant concentration is maintained. Further, a sol-gel approach promotes the low-temperature synthesis of materials that are generally of higher purity and of greater compositional flexibility than those attainable by conventional crystal-growing or melt-quenching (for glasses) techniques. We describe the synthesis and luminescence properties of Pr^{3+}- and Dy^{3+}-doped lanthanum halide powders by a sol-gel approach coupled with reactive-atmosphere processing. Luminescence spectra and fluorescence lifetimes for the 1.3-μm transitions of these dopants are given and discussed in reference to melt-derived, single-crystal analogs.

The synthesis of the lanthaum halides was accomplished by a two-step process. First, $LaCl_3 \cdot 6H_2O$ (Johnson-Matthey, Ward Hill, Mass.) was dissolved in triply deionized water. Doped samples were synthesized by the addition of $PrCl_3 \cdot 6H_2O$ or $DyCl_3 \cdot 6H_2O$ to the aqueous $LaCl_3$ solution. Excess NH_4OH was added to precipitate $La(OH)_3$ out of solution. These samples subsequently were washed in triply deionized water to remove the soluble ammonium chloride reaction by-product and dried at 90 °C for 24 h. Then the samples were transferred to an alumina muffle-tube furnace (CM Furnace Company, Bloomfield, N.J.) for reactive-atmosphere processing. The sealed furnace was purged with nitrogen gas (liquid-nitrogen source) and heated to temperature at 10 °C/min. Anhydrous hydrogen fluoride or hydrogen chloride (both 99.99% pure; Matheson Gas Products, East Rutherford, N.J.) was subsequently introduced into the nitrogen flow, providing conversion of the lanthanum hydroxide into the respective lanthanum halide (~500 cm^3/min HF or HCl, ~ 500 cm^3/min nitrogen gas). Reactive atmosphere processing lasted 1 h, after which the reactive gas was turned off and the furnace was cooled to room temperature under flowing nitrogen.

X-ray diffraction analysis was performed with a D500 diffractometer (Siemens Industrial Automation, Inc., Madison, Wis.) using nickel-filtered CuK_α radiation. Fluorescence measurements were made with a tunable Ti:sapphire laser (Schwartz-Electro Optics, Orlando, Fla.,) excited by an argon-ion laser (I-200; Coherent, Torrance, Calif.). The pump beam was mod-

0146-9592/97/100691-03$10.00/0

ulated with a chopper (EG&G Model 196; Princeton Applied Research, Princeton, N.J.) at 40 Hz, with sample emissions collected by an InGaAs detector (Electro-Optical Systems, Pheonixville, Pa.) at 90° to the direction of the pump.

Sol-gel-derived Pr^{3+}- and Dy^{3+}-doped LaF_3 and $LaCl_3$ were produced successfully by reactive-atmosphere treatments of hydroxide powders. X-ray diffraction standards[7] were used to verify synthesis of the respective halides.[8]

Fluorescence at 1.3 μm from the 750-parts-in-10^6 (ppm) Pr^{3+}-doped LaF_3 sample, treated at 600 °C, is shown in Fig. 1. Excitation at 1.017 μm by the Ti:sapphire laser populates the $^1G_4$ level of the Pr^{3+} ion, which emits at 1.3 μm upon radiative decay to the $^3H_5$ state. The 3-dB bandwidth is ~100 nm (1280 nm → 1380 nm), with peak asymmetry attributed to crystal-field effects. The lifetime for this emission was 0.23 ms (Table 1). Figure 2 shows the fluorescent emission at 1.3 μm from a 500-ppm Pr^{3+}-doped $LaCl_3$ sample. The effects of crystal-field symmetry are clearly evident, with a maximum peak intensity occurring at ~1315 nm. The emission, although it is spectrally uneven, is broadband, ranging from 1290 to 1400 nm. Lifetimes for the 200 °C chlorinated samples were of the order of 1 ms, with a slight increase if chlorination occurred at 400 °C. Luminescence from the $(^6H_{9/2}, {}^6F_{11/2}) \rightarrow {}^6H_{15/2}$ transition of Dy^{3+}:$LaCl_3$ (500 ppm) is shown in Fig. 3. Excitation by the Ti:sapphire laser occurred at 810 nm. A 45-nm (1295 nm → 1345 nm) 3-dB bandwidth is observed, with a characteristic three-peak spectral feature.[9] Radiative lifetimes for the 500-ppm samples were greater then 1.1 ms, again increasing when the chlorination temperature was raised from 200 to 400 °C.

The radiative quantum efficiency from the $^1G_4$ level of Pr^{3+}:LaF_3 can be determined by comparison of the 0.23-ms measured lifetime (750-ppm Pr^{3+}:LaF_3 by sol-gel) with that calculated by Weber[10] following Judd–Ofelt analysis of Pr^{3+}-doped LaF_3 single crystals. In this case the quantum efficiency is

$$\eta = \frac{\tau_{LaF_3}}{\tau_c} = \frac{0.23}{3.11} \cong 8\%,$$

where 0.23 ms (τ_{LaF_3}) is the measured lifetime of the 1.3-μm emission from the HF600 sample (abbreviations explained in Table 1) and the 3.11-ms theoretical lifetime (τ_c) is the reciprocal of the $\Sigma A(^1G_4, J_j)$ value given by Weber.[10] This efficiency is approximately one half of the theoretical efficiency calculated from tabulated spontaneous-emission probabilities and multiphonon emission rates.[8] Absorbed OH^- is known to quench the $^1G_4$ lifetime[11]; therefore it is likely that this phenomenon accounts for the less-than-theoretical quantum efficiency value, as samples had not been isolated from the atmosphere. Fourier-transform infrared analysis of the sol-gel-derived powders indicated the existence of residual OH species; however, the portion attributed to surface water has not been quantified. To a lesser extent, the 750-ppm Pr^{3+} concentration is high enough that we should expect some nonradiative cross relaxations between neighboring ions.[12]

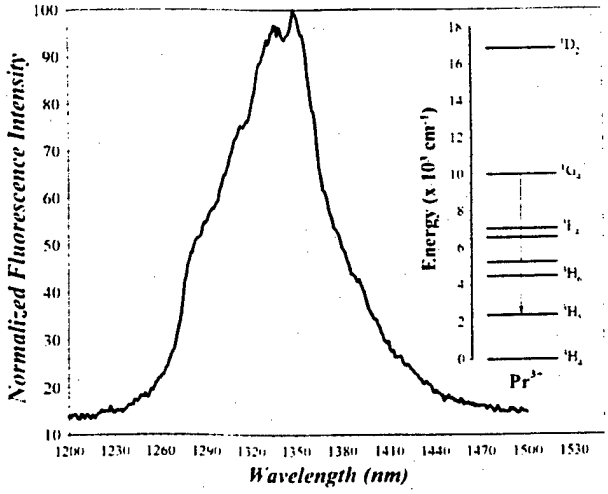

Fig. 1. Normalized fluorescence spectra for sol-gel-derived LaF_3 doped with 750-ppm Pr^{3+}. Inset: Pr^{3+} energy-level diagram, with the 1.3-μm transition indicated by the arrow.

Table 1. Measured Lifetimes and Calculated Radiative Quantum Efficiencies for 1.3-μm Emissions

Sample[a]	Lifetime (ms)	Quantum Efficiency (%)
750-ppm Pr:LaF_3 HF600	0.23	8
500-ppm Pr:$LaCl_3$ HCl200	0.97	66
500-ppm Pr:$LaCl_3$ HCl400	1.06	72
500-ppm Dy:$LaCl_3$ HCl200	1.11	68
500-ppm Dy:$LaCl_3$ HCl400	1.31	78

[a]The abbreviations refer to halide gas and temperature; e.g., HF600 corresponds to anhydrous HF gas at 600 °C. All treatments lasted for 1 h. Lifetime values correspond to the first e-folding time [i.e., the time for luminescence intensity to fall to $\exp(-1)$ of its original value].

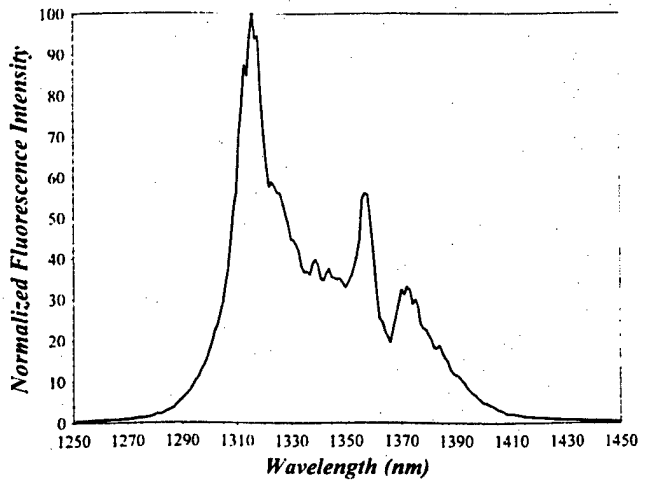

Fig. 2. Normalized fluorescence spectra for sol-gel-derived $LaCl_3$ doped with 500-ppm Pr^{3+}.

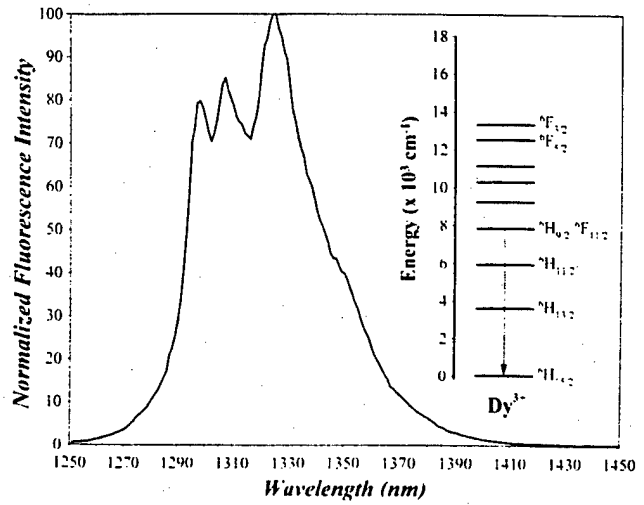

Fig. 3. Normalized fluorescence spectra for sol-gel-derived $LaCl_3$ doped with 500-ppm Dy^{3+}. Inset: Dy^{3+} energy-level diagram, with the 1.3-μm transition indicated by the arrow.

The 260-cm^{-1} phonon energy of $LaCl_3$ implies an extremely low nonradiative relaxation rate and hence a potential radiative quantum efficiency of 100% from the $^1G_4$ level.[8] The sol-gel-derived $LaCl_3$ exhibited radiative lifetimes of 0.97 and 1.06 ms when it was processed with anhydrous HCl for 1 h at 200 and 400 °C, respectively. These values correspond to quantum efficiencies of

$$\eta = \left(\frac{\tau_{200}}{\tau_c}\right) \times 100 = \left(\frac{0.97}{1.466}\right) \times 100 = 66\% ,$$

$$\left(\frac{\tau_{400}}{\tau_c}\right) \times 100 = \left(\frac{1.06}{1.466}\right) \times 100 = 72\% .$$

The 1.466-ms theoretical lifetime was calculated from the electric and magnetic dipole radiative rates following Judd–Ofelt analysis of Pr^{3+}:$LaCl_3$ single crystals.[13]

The spectroscopic properties of the sol-gel-derived Dy^{3+}:$LaCl_3$ samples with respect to melt-grown single crystals are in close agreement. The lifetimes measured for sol-gel Dy^{3+}:$LaCl_3$ were 1.11 ms (HCl200) and 1.31 ms (HCl400). Judd–Ofelt analysis by Page *et al.*[14] yielded a theoretical radiative lifetime of 1.68 ms from the ($^6H_{9/2}$, $^6F_{11/2}$) excited-state manifold. Correspondingly, the sol-gel quantum efficiencies are 66% (HCl200) and 78% (HCl400). The efficiency of the HF200 sample compares favorably with the 68% efficiency measured for single crystals grown (3 mm/h) at 880 °C.[14]

Highly efficient luminescence at 1.3 μm has been observed, for the first time to our knowledge, from sol-gel-derived materials. Comparison of these hosts with doped single crystals indicates equivalent spectroscopic performance at a greatly reduced synthesis temperature. Active devices produced by a process such as sintering of the halide powders are envisaged for the future. The versatility, ease, and low cost of this sol-gel process represent significant advances in the synthesis of highly efficient 1.3-μm fluorescent materials for both optical fiber amplifiers and thin-film amplifiers for planar integrated photonics.

References

1. E. Kreifeldt, Opt. Photon. News **7**(6), 8 (1996).
2. C. A. Brackett, J. Lightwave Technol. **14,** 986 (1996).
3. K. Lewotsky, Laser Focus World **32**(7), 43 (1996).
4. Y. Ohishi, T. Kanamori, T. Kitagawa, S. Takahashi, E. Snitzer, and G. H. Sigel, Jr., Opt. Lett. **16,** 1747 (1991).
5. T. J. Whitley, J. Lightwave Technol. **13,** 744 (1995).
6. S. Tanabe, T. Hanada, M. Watanabe, T. Hayashi, and N. Soga, J. Am. Ceram. Soc. **78,** 2917 (1995).
7. Joint Committee on Powder Diffraction Standard: 8-461 (LaF_3) and 12-605 ($LaCl_3$).
8. J. Ballato, "Sol-gel synthesis of rare-earth-doped halide optical materials for photonic applications," Ph.D. dissertation (Rutgers University, Piscataway, N.J., 1997).
9. R. H. Page, K. I. Schaffers, G. D. Wilke, P. A. Waide, J. B. Tassano, R. J. Beach, and S. A. Payne, in *Optical Fiber Communication Conference*, Vol. 8 of 1996 OSA Technical Digest Series (Optical Society of America, Washington, D.C., 1996), paper TuG2.
10. M. J. Weber, J. Chem. Phys. **48,** 4774 (1968).
11. A. J. Faber, D. R. Simons, Y. Yan, and H. de Waal, Proc. SPIE **2290,** 80 (1994).
12. Y. Ohishi, T. Kanamori, T. Nishi, and S. Takahashi, IEEE Photon. Technol. Lett. **3,** 715 (1991).
13. L. B. Shaw, S. R. Bowman, B. J. Feldman, and J. Ganem, IEEE J. Quantum Electron. **32,** 2166 (1996).
14. R. H. Page, K. I. Scaffers, S. A. Payne, and W. F. Krupke, "Dy-doped chlorides as gain media for 1.3 μm telecommunications amplifiers," J. Lightwave Technol. (to be published).

The increase in crosstalk at frequencies beyond 2GHz probably result from the capacitive coupling through the parasitics in the array. The use of separate bias sources eliminates the feedback path from the amplifier, through the power line, to the input of the photodiode, thus resulting in > 10dB reduction in crosstalk. For long distance fibre-optic communication, sensitivity plays an important role in the overall performance. Measurement of this parameter is in progress.

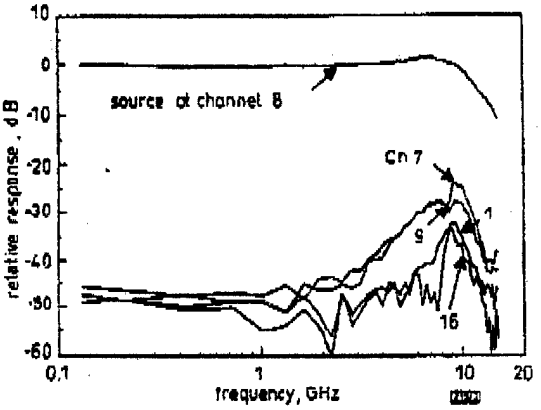

Fig. 3 *Crosstalk characteristics of dual biased integrated 16-channel photoreceiver array with channel eight photoexcited*

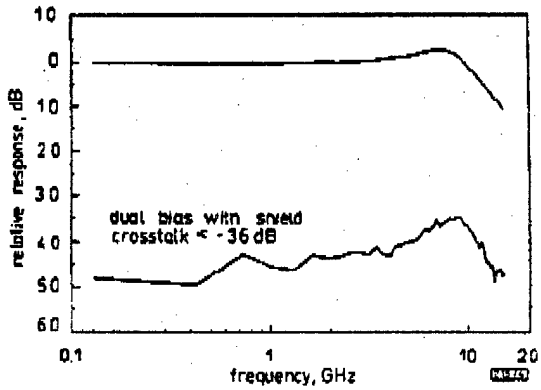

Fig. 4 *Adjacent channel crosstalk with both dual bias design and incorporation of metal shield*

In summary, we demonstrate a 16-channel *pin*/HBT monolithically integrated photoreceiver array with 11.5GHz bandwidth per channel and adjacent channel crosstalk < –35dB.

Acknowledgments: The authors acknowledge the help provided by A.L. Gutierrez-Aitken. This work is supported by the Defense Advanced Research Projects Agency, Grant MDA 972-94-1-0004, and US Army Research Office, Grant DAALO3-92-G-0109.

20 October 1996
Electronics Letters Online No: 19970029

K.-C. Syao, K. Yang, X. Zhang, G.I. Haddad and P. Bhattacharya (*Solid State Electronics Laboratory, Department of Electrical Engineering and Computer Science, The University of Michigan, Ann Arbor, Michigan 48109-2122, USA*)

References

1 AOA, K., YANO, H., MURATA, M., KAMEI, H., SASAKI, G., and HAYASHI, H.: '5Gbit/s eight-channel optoelectronic integrated receiverarrays comprising GaInAs pin PDs and AlInAs/GaInAs HEMTs', Tech. Dig., Opt. Fiber Comm. Conf. (OFC'91), San Diego, February 1991, CA Paper TuB2

2 CHANDRASEKHAR, S., GARRETT, L.D., LUNARDI, L.M., DENTAI, A.G., BURRUS, C.A., and BURROWS, E.C.: 'Investigation of crosstalk performance of eight-channel pin/HBT OEIC photoreceiver array modules', *IEEE Photonics Technol. Lett.*, 1996, 8, pp. 682–684

3 LEE, W.S., SPEAR, D.A.H., SMITH, A.D., WHEELER, S.A., and BLAND, S.W.: 'Monolithic eight-channel photoreceiver array OEICs for HDWDM applications at 1.55μm', *Electron. Lett.*, 1992, 28, pp. 612–614

4 YANO, H., SASAKI, G., NISHIYAMA, N., MURATA, M., KAMIYAMA, H., and HAYASHI, H.: '5Gbit/s four-channel receiver optoelectronic integrated circuit array for long-wavelength lightwave systems', *Electron. Lett.*, 1992, 28, pp. 503–504

5 YANG, K., GUTIERREZ-AITKEN, A.L., ZHANG, X., HADDAD, G.I., and BHATTACHARYA, P.: 'Design, modelling, and characterization of monolithically integrated InP-based (1.55μm) high-speed (24GB/s) p-i-n/HBT front-end photoreceivers', *J. Lightwave Technol.*, 1996, 14, pp. 1831–1839

6 GUTIERREZ-AITKEN, A.L., COWLES, J.C., BHATTACHARYA, P.K., and HADDAD, G.I.: 'High bandwidth InAlAs/InGaAs PIN-HBT monolithic integrated photoreceiver', Proc. 6th Int. Conf. InP and Rd. Mat., 1994, pp. 247–250

7 GUTIERREZ-AITKEN, A.L., BHATTACHARYA, P., SYAO, K.-C., YANG, K., HADDAD, G.I., and ZHANG, X.: 'Low crosstalk (< –40dB) in 1.55μm high speed OEIC photoreceiver arrays with novel on-chip shielding', *Electron. Lett.*, 1996, 32, pp. 1706–1708

Electronics Letters, 33, p. 83–84 (1997)

Patterning for planar waveguides

J. Ballato, R. van Weeren, M. Agarwala, R.E. Riman and S.C. Danforth

Indexing term: Planar waveguides

The synthesis of planar strip geometries for planar waveguides by a layered manufacturing technique, called fused deposition modelling (FDM™), is presented. Channels were deposited on silicon wafers by melting a thermoplastic polymer and extruding it through a small orifice. Sol-gel-derived, amorphous fluoride films were dip-coated into these channels and yielded straight, 1mm strips on subsequent removal of the polymer.

Introduction: The future demand of the 'information superhighway' has manifested intense interest in the development of new planar photonic materials and waveguiding geometries. The integration of optics and electronics into single devices has even been likened to the creation of the transistor in terms of its technological significance [1]. In light of this, the photonic device market is projected to grow from the current multimillion dollar per year industry into one valued at several billion dollars per year by 2010 [2].

Planar waveguide geometries inevitably will play an extensive role in optoelectronic devices. Integration increases functionality with fewer components and at a lower level of power consumption. Consequently, applications are bound for both passive and active applications. At times, the majority of the expenses are incurred in the packaging of the device rather than in the preparation of the constituent materials. Therefore, overcoming the current technological barrier of high packaging costs would represent an additional advantage for photonic devices. We report the novel synthesis of planar glass strips by a rapid prototyping, layered manufacturing method. Such techniques are quickly gaining industrial interest as fabrication tools, since they reduce production times and costs, as well as providing easy testing of new and complex design geometries. The great simplicity and flexibility of this technology is advantageous to the expeditious realisation of novel prototype waveguiding structures for planar photonic applications.

Film synthesis and patterning: The patterns were fabricated on single-crystal silicon wafers using a commercial rapid prototyping (RP) process called fused deposition modelling (FDM™). All RP processes have the initial design of the part or pattern on a CAD workstation in common. The design is mathematically sliced into a finite number of horizontal layers of certain thicknesses. These parts then are fabricated, layer-by-layer, by the specific RP hardware. The process by which each RP technique fabricates these individual layers differs significantly. In the FDM™ process, the layers are fabricated by extrusion of a molten thermoplastic

aterial through a fine nozzle. The extrudate is deposited as continuous lines ('roads') of material, only in areas defined by the CAD file for each layer, or slice. The extruded material solidifies apidly upon deposition. The motion of the extrusion head (liquifier) is controlled in the x, y direction while a support platform rovides the z motion.

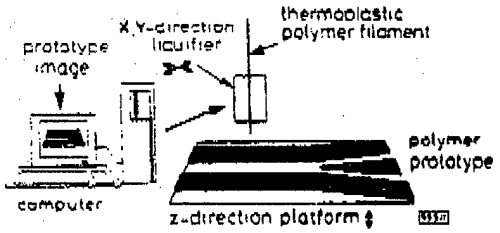

ig. 1 *Schematic diagram of rapid prototyping synthesis of planar glass trips by fabricating wax patterns by FDM™*

Subsequent to the deposition of the polymer pattern, the Si afer was dipcoated with a sol containing the cationic precursors f a ZBLA (57 ZrF_4-36 BaF_2-4 LaF_3-3 AlF_3) fluoride glass [3]. Following gelation in air at room temperature, a heat treatment at 0°C for 1h was sufficient to melt the wax off the substrate. A hematic diagram of this type of process is shown in Fig. 1. Conersion of the glass to a fluoride was achieved by a 1h, 200°C eatment in anhydrous HF. The present work was concerned with e synthesis of patterned fluoride films. Waveguides could easily based on a variety of materials such as oxides which are proced by various methodologies such as sol-gel or ion exchange.

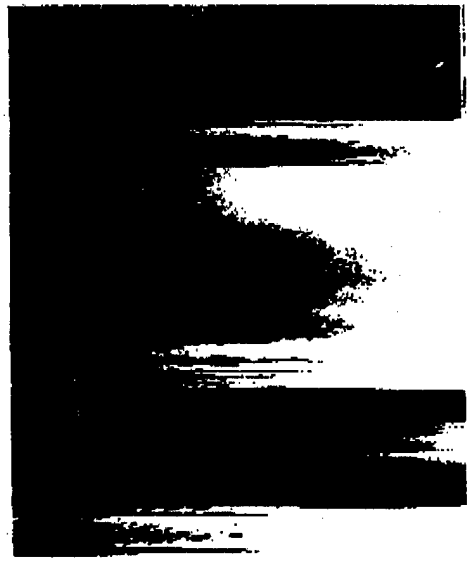

ig. 2 *Optical micrograph of FDM fluoride glass strips*
uide width is 1mm

iscussion: The resultant planar glass strips are shown in Fig. 2. he fringes observed at the strip edges are the result of surface nsion effects between the sol and the wax. As film thicknesses e increased, these effects should become less problematic. Also bserved in the Figure are bubbles in the glass regions. These cur from the deposition of the sol which gelled too quickly to ow the bubbles by buoyancy. Control of the gelation conditions g., considering sol-gel methods: alcohol dilution of sol, or coatg under an alcohol/water atmosphere) should allow for crackd bubble-free films.

An important point to note is the straightness of the guide ges. Irregularities in either these borders or on the major surces quickly lead to high scattering losses. The ability to fabricate ges of this regularity confirm the feasibility of this method to oduce quality waveguides. As mentioned, the nonuniformity in e top surface resulted from non-optimised processing of the sol-derived film. However, this currently is of less concern than the character of the edges, as sol-gel methods have been shown to yield highly smooth films [4].

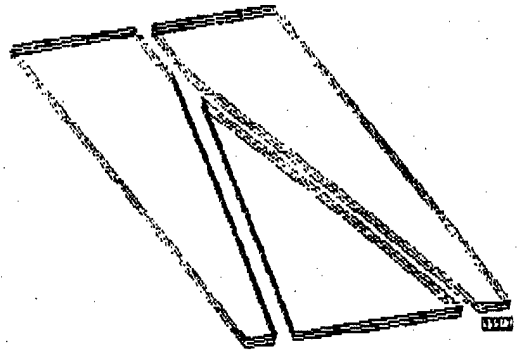

Fig. 3 *Example of potential structure to be synthesised*
This corresponds to CAD projection of planar Y-branch
Geometry is converted into instructions which control the 3D location of extrusion die with respect to substrate

Rapid prototyping techniques are increasingly receiving greater attention as industry realises their benefits. Potential lies in the untapped field of planar devices for integrated photonics. Our present resolutions are of the order of 25μm, mostly due to mechanical limitations of the FDM system (e.g., control hardware and software, nozzle size, etc.). Although this causes a restriction to larger-scale applications (such as planar sensors), the future holds promise for a continued advance in the patterning of smaller features. Further, the ability to deposit several materials at the same time, coupled with simplicity and design flexibility (as shown in Fig. 3), enhances the utility of this technique.

Conclusions: We have shown the feasibility of layered manufacturing to produce uniform structures of interest to planar photonic devices. This synthesis method is applicable to an extremely wide range of geometries which are quickly and easily fabricated. This expediency greatly reduces processing costs, especially those associated with design optimisation based on the performance of prototypes.

Acknowledgment: The authors wish to thank G. Walker for his valuable computer skills.

2 October 1996
Electronics Letters Online No: 19970034

J. Ballato, R. van Weeren, M. Agarwala, R.E. Riman and S.C. Danforth (*Rutgers, The State University of New Jersey, Department of Ceramic Science and Engineering, Brett & Bowser Roads, Piscataway, NJ 08855-0909, USA*)

References

1 HIGGINS, T.V.: 'Optoelectronics: The next technological revolution', *Laser Focus World*, November 1995
2 GOODMAN, M.S., and ARTHURS, E.: 'Telecommunications system applications for optoelectronic integrated circuits' *in* DEGANAIS, M., LEHENY, R.F., and CROW, J. (Eds.): 'Integrated optoelectronics' (Academic Press, New York, 1995), pp. 3–29
3 BALLATO, J., DEINEKA, M., RIMAN, R.E., SNITZER, E., and ZHOU, W.: 'Sol-gel synthesis of rare-earth-doped fluoride glass thin films', *J. Mater. Res.*, 1996, 11, pp. 841–849
4 DU, X.M., ORIGNAC, X., and ALMEIDA, R.M.: 'Striation-free, spin-coated sol-gel optical films', *J. Am. Ceram. Soc.*, 1995, 78, pp. 2254–2256

ELSEVIER

Journal of Non-Crystalline Solids 215 (1997) 113–124

JOURNAL OF NON-CRYSTALLINE SOLIDS

High-temperature calorimetric study of glass-forming fluorozirconates

I-Ching Lin [a,*], Alexandra Navrotsky [a], John Ballato [b], Richard E. Riman [b]

[a] *Princeton Materials Institute and Department of Geosciences, Princeton University, Princeton, NJ 08544, USA*
[b] *Department of Ceramics, Rutgers University, Piscataway, NJ 08854, USA*

Received 21 August 1996; revised 13 January 1997

Abstract

Using high temperature calorimetric techniques, enthalpies of mixing of melts, enthalpies of formation of glasses and enthalpies of formation of crystals have been measured in binary systems ZrF_4–BaF_2, ZrF_4–NaF, ZrF_4–LaF_3 and selected compositions in the system ZrF_4–BaF_2–LaF_3–AlF_3–NaF. The system ZrF_4–LaF_3 shows essentially zero enthalpies of mixing of melts. In the other systems, there are strongly exothermic enthalpies of mixing. In the binary systems ZrF_4–BaF_2 and ZrF_4–NaF, the enthalpy of mixing of melts and the enthalpy of formation of crystals show minima at the same compositions, Ba_2ZrF_8 and Na_3ZrF_7, respectively, indicating the stoichiometric complexes ZrF_8^{4-} and ZrF_7^{3-}. These results are discussed in relation to energetics, structure, speciation and acid–base chemistry and suggest the following: ZrF_4, LaF_3 and AlF_3 are anionic complex-formers, while BaF_2 and NaF are ionized in the molten state. The coordination number of the zirconium fluoride anionic complex varies with the amount of alkali or alkaline earth fluoride. A model is proposed in which glass-forming melts are dominated by ZrF_5^- species and lie near deep eutectics. Therefore, glass formation in fluorozirconates involves a substantial structural change, which is dominated by short-range atomic arrangements, from the melt with predominantly ZrF_5^- to the glass where zirconium is 7 or 8 coordinated by fluorine. © 1997 Elsevier Science B.V.

PACS: 05.70.– a; 07.20.Fw; 61.20.Qg; 61.43.Fs

1. Introduction

Heavy metal fluoride glasses based on ZrF_4 (fluorozirconate glasses) have been studied extensively for more than 15 years because of their potential for optical applications [1–4]. The addition of other fluorides to the binary system ZrF_4–BaF_2 improves the apparent ease of glass formation and gives a series of multicomponent fluoride glasses. ZBLAN (ZrF_4–BaF_2–LaF_3–AlF_3–NaF) glasses appear to be the most stable against devitrification and are the most commonly studied. Their generally accepted structure is made up of ZrF_7 and ZrF_8 polyhedra bonded by one or two bridging fluorine atoms. Cations, such as Ba^{2+} and Na^+, are inserted among the polyhedra [5–8].

Glass-forming compositions have been found empirically in fluorozirconate systems. No completely satisfactory explanation has been provided for glass formation. Fluorozirconate glasses are mainly formed by supercooling their melts. Thus, a understanding of properties in the molten state must be considered to

* Corresponding author. Tel.: +1-609 258 3287; fax: +1-609 258 1274; e-mail: iclin@phoenix.princeton.edu.

PII S0022-3093(97)00081-1

analyze glass formation. It is known that fluorozirconate melts have low viscosities when compared with common glass-forming systems such as silicates and borates [9–12] and are typically 'fragile' glass-forming liquids [13]. However, due to the high vapor pressure and corrosive nature of ZrF_4, few thermodynamic studies have been performed by high temperature calorimetry. The enthalpies of mixing of molten ZrF_4–BaF_2 (ZB), ZrF_4–NaF (ZN) and ZrF_4–BaF_2–NaF (ZBN) mixtures have been measured and found to be exothermic [14–18]. These data were interpreted in terms of zirconium fluoride anionic complex formation in the molten state. Several spectroscopic investigations have confirmed the occurrence of anionic complexes in melts [19–22].

The thermodynamic parameter, enthalpy, is a useful tool which gives insights into structure and bonding when analyzed systematically for a group of materials. The goals of this work are to obtain reliable thermodynamic data including the enthalpies of mixing of melts, the enthalpies of formation of glasses and the enthalpies of formation of crystals in fluorozirconate systems and to develop systematic knowledge relating energetics, structure, speciation, acid–base chemistry, physical properties and ease of glass formation.

2. Experimental

2.1. Synthesis and characterization

High-purity fluorides (i.e., ZrF_4, BaF_2, LaF_3, AlF_3 and NaF) were used as starting materials. All chemicals were stored and handled in a dry box to prevent hydroxide and oxide contamination. ZB, ZL and ZBN glasses were prepared by melting the batches in sealed platinum tubes at 950–1050°C for 1 h. Vitreous transparent pieces of thickness 1–2 mm were obtained by fast quenching the tubes in water. Glassy samples of ZBL, ZBA, ZBLA and ZBLAN were prepared by splat cooling fluorozirconate melts. The compositions of all glasses were confirmed by wavelength dispersive electron microprobe analyses. The melting and cooling schedules used for preparation of the crystalline phases were either those described in the literature [23,24] or were based on their phase diagrams [25–27]. The synthesized crystalline compounds were identified by X-ray powder diffraction (XRD). Most were the expected single phases, with diffraction patterns in good agreement with PDF (power diffraction file) cards. Crystalline $LaZr_2F_{11}$ in this study is the meta-$LaZr_2F_{11}$ phase reported to be stable over the whole temperature range [28]. α-$BaZr_2F_{10}$, β-$BaZr_2F_{10}$ and crystalline ZBLAN (0.53–0.21–0.04–0.03–0.19) samples were recrystallized by heating the corresponding glasses. XRD patterns for both α-$BaZr_2F_{10}$ and β-$BaZr_2F_{10}$ show a large number of lines, indicating the probable presence of other phases. The more-intense lines could be attributed to α-$BaZr_2F_{10}$ and β-$BaZr_2F_{10}$. It was not possible to identify other phases from the remaining diffraction lines. The great difficulty in obtaining these phases has been reported previously [29,30]. The major phase in the recrystallized ZBLAN was identified as $BaNaZr_2F_{11}$. Some glassy samples were annealed at temperatures 10–20°C below their glass transition temperatures for 30 min and then cooled at 1°C/min to room temperature in order to compare energetic differences between fast cooling and annealing.

2.2. Calorimetry

Enthalpy measurements were made by transposed-temperature-drop calorimetry using a high temperature hybrid calorimeter constructed in the calorimetry laboratory at Princeton University [31]. This custom-built calorimeter combines the advantages of the Calvet twin and Setaram HT-1500 calorimeters [32]. It can be operated at any selected temperature between 600 and 1000°C. All samples, each weighing about 60–90 mg, were sealed in Au-capsules due to the hygroscopic nature of ZrF_4 and glasses at low temperature and the high vapor pressure and the corrosive nature of ZrF_4-based melts at high temperature. The sealed Au-capsules were dropped from room temperature into the calorimeter at 800 or 900°C, depending on their compositions. Calibration was done by dropping known masses of platinum, and showed two standard deviations of the mean of 1–2%.

2.3. Thermodynamic cycles

After subtracting the heat content of the Au-capsule, the data were analyzed by different thermodynamic cycles. In the text, the states of liquid, crystal and glass are symbolized by subscripts, liq, xl and

gl; respectiv
for fluoride
sured enthal
($\Delta H_{drop}^{mixture}$))
mixing of m
ing, ΔH_{mix})
example, the
of drop of C
tion:

$0.25BaF_{2(xl.}$

$\rightarrow$ (0.25E

By using
effects of th

$0.25BaF_{2(xl.}$

$\rightarrow 0.25Ba$

$0.75ZrF_{4(xl.2}$

$\rightarrow 0.75Zr$

$0.25BaF_{2(xl.}$

$\rightarrow 0.25Ba$

$0.75ZrF_{4(xl.8}$

$\rightarrow 0.75Zr$

For each
difference in

Table 1
Thermodynamic
[33–35]

Fluoride	T_m (°C)
ZrF_4	93
BaF_2	136
LaF_3	149
AlF_3	225
NaF	996

T_m: melting tem
ing temperature.
$H_{25°C}$: heat cont
temperature.

gl, respectively. By using the thermodynamic data for fluoride components (Table 1) [33–35], the measured enthalpies for the drop of mechanical mixtures ($\Delta H_{drop}^{mixture}$)) were converted to give the enthalpies of mixing of melts (i.e., liquid–liquid enthalpy of mixing, ΔH_{mix}) at the experimental temperature. For example, the experimental measurement for enthalpy of drop of $0.25BaF_2 \cdot 0.75ZrF_4$ mixture is the reaction:

$$0.25BaF_{2\,(xl.25°C)} + 0.75ZrF_{4\,(xl.25°C)} \rightarrow (0.25BaF_2 \cdot 0.75ZrF_4)_{(liq.800°C)} \quad \Delta H_{drop}^{mixture}.$$

By using the thermodynamic data in Table 1, heat effects of the following reactions are calculated:

$$0.25BaF_{2\,(xl.25°C)} \rightarrow 0.25BaF_{2\,(xl.800°C)} \quad (H_T - H_{25°C})_{BaF_2},$$

$$0.75ZrF_{4\,(xl.25°C)} \rightarrow 0.75ZrF_{4\,(xl.800°C)} \quad (H_T - H_{25°C})_{ZrF_4},$$

$$0.25BaF_{2\,(xl.800°C)} \rightarrow 0.25BaF_{2\,(liq.800°C)} \quad \Delta H_{fus(T)BaF_2},$$

$$0.75ZrF_{4\,(xl.800°C)} \rightarrow 0.75ZrF_{4\,(liq.800°C)} \quad \Delta H_{fus(T)ZrF_4}.$$

For each fluoride component, $H_T - H_{25°C}$ is the difference in enthalpy between the experimental temperature and 25°C in the solid state, also called the heat content. $\Delta H_{fus(T)} = \Delta H_{fus(T_m)} + \int_{T_m}^{T} \Delta C_p \, dT$ ($T < T_m$), where $\Delta H_{fus(T)}$ is the enthalpy of fusion at the experimental temperature (T) and $\Delta H_{fus(T_m)}$ is the enthalpy of fusion at the melting point (T_m). $\int_{T_m}^{T} \Delta C_p \, dT$ is the difference between $\Delta H_{fus(T)}$ and $\Delta H_{fus(T_m)}$ and is obtained by integration of the difference between the extrapolated heat capacity of liquid and the heat capacity of solid from T_m to T. Finally, the enthalpy of mixing of the molten $0.25BaF_2 \cdot 0.75ZrF_4$ at 800°C, i.e., the heat of the following reaction:

$$0.25BaF_{2\,(liq.800°C)} + 0.75ZrF_{4\,(liq.800°C)} \rightarrow (0.25BaF_2 \cdot 0.75ZrF_4)_{(liq.800°C)} \quad \Delta H_{mix}$$

can be obtained, where $\Delta H_{mix} = \Delta H_{drop}^{mixture} - (H_T - H_{25°C})_{BaF_2} - (H_T - H_{25°C})_{ZrF_4} - \Delta H_{fus(T)BaF_2} - \Delta H_{fus(T)ZrF_4}$.

For the enthalpy of formation of the glasses and crystals having lower liquidus temperatures than the experimental temperatures, for example, crystalline $BaZr_2F_{10}$ which melts at 590°C [27], the thermodynamic cycle is

$$1/3BaF_{2\,(xl.25°C)} + 2/3ZrF_{4\,(xl.25°C)} \rightarrow (1/3BaF_2 \cdot 2/3ZrF_4)_{(liq.800°C)} \quad \Delta H_{drop}^{mixture},$$

$$1/3BaZr_2F_{10\,(xl.25°C)} \rightarrow (1/3BaF_2 \cdot 2/3ZrF_4)_{(liq.800°C)} \quad \Delta H_{drop}^{crystal}.$$

The final states are the same in both reactions. The difference between two reactions gives

$$1/3BaF_{2\,(xl.25°C)} + 2/3ZrF_{4\,(xl.25°C)} \rightarrow 1/3BaZr_2F_{10\,(xl.25°C)} \quad \Delta H_{form}^{crystal}.$$

$\Delta H_{form}^{crystal} = \Delta H_{drop}^{mixture} - \Delta H_{drop}^{crystal}$, where $\Delta H_{form}^{crystal}$, is the enthalpy of formation of $1/3(BaZr_2F_{10})$ from the crystalline fluorides at 25°C. $\Delta H_{drop}^{mixture}$ was either directly measured or calculated by interpolating the experimental measurements.

The enthalpy of formation of crystals, which have higher melting temperatures than the experimental calorimetric temperature, was determined by a method similar to that used for the enthalpy of formation of $NaMgF_3$ [36]. This method converts both reactants and product to the same final molten state, by dropping a mixture of reactants plus an

Table 1
Thermodynamic data for fluoride components used in this study [33–35]

Fluoride	T_m (°C)	$H_{fus(T_m)}$ (kJ/mol)	T (°C)	$H_T - H_{25°C}$ (kJ/mol)	$H_{fus(T)}$ (kJ/mol)
ZrF_4	932	64.22	900	110.27	65.24
			800	96.60	68.32
BaF_2	1368	20.92	900	79.36	39.20
			800	67.68	40.98
LaF_3	1493	50.21	900	92.16	31.73
			800	80.04	27.12
AlF_3	2250	98.30	800	74.77	73.69
NaF	996	33.35	900	49.09	32.84
			800	42.81	32.15

T_m: melting temperature. $H_{fus(T_m)}$: enthalpy of fusion at the melting temperature. T: experimental calorimetric temperature. $H_T - H_{25°C}$: heat content. $H_{fus(T)}$: enthalpy of fusion at the experimental temperature.

excess component to produce a low-melting final composition. For example, the measurement for enthalpy of formation of Ba_2ZrF_8, which melts congruently at 1016°C [27], is

$$1/3BaF_{2\,(xl.25°C)} + 2/3ZrF_{4\,(xl.25°C)} \rightarrow (1/3BaF_2 \cdot 2/3ZrF_4)_{(liq.800°C)} \quad \Delta H_{drop}^{mixture},$$

$$1/6Ba_2ZrF_{8\,(xl.25°C)} + 1/2ZrF_{4\,(xl.25°C)} \rightarrow (1/3BaF_2 \cdot 2/3ZrF_4)_{(liq.800°C)} \quad \Delta H_{drop}^{crystal}.$$

The final states are the same in both reactions. The difference between two reactions gives

$$1/3BaF_{2\,(xl.25°C)} + 1/6ZrF_{4\,(xl.25°C)} \rightarrow 1/6Ba_2ZrF_{8\,(xl.25°C)} \quad \Delta H_{form}^{crystal}.$$

$\Delta H_{form}^{crystal} = \Delta H_{drop}^{mixture} - \Delta H_{drop}^{crystal}$ and $2\,\Delta H_{form}^{crystal}$ is the enthalpy of formation of $1/3(Ba_2ZrF_8)$ from the crystalline fluorides at 25°C. All calorimetric data are based on one mole of fluoride, i.e., the number of total moles of components is 1.

3. Results

Calorimetric data for mixtures, glasses and crystals are listed in Tables 2–4, respectively. The enthalpies of mixing of molten mixtures (i.e., liquid–liquid heat of mixing, ΔH_{mix}) at 800°C for ZrF_4–BaF_2 and at 900°C for ZrF_4–NaF and ZrF_4–LaF_3 are shown as circles in Fig. 1. In the system ZrF_4–BaF_2, a third-order polynomial fit to the data provides the enthalpy of mixing curve. In the systems ZrF_4–NaF and ZrF_4–LaF_3, the enthalpy of mixing curves are interpolated from the data. These are shown as the dashed curves in Fig. 1. The enthalpies of formation of glasses and crystals from the crystalline fluorides at 25°C (ΔH_{form}^{glass} and $\Delta H_{form}^{crystal}$) are shown as triangles and squares, respectively, in Fig. 1.

The enthalpy of mixing in the system ZrF_4–BaF_2 has been obtained by Hatem et al. at 750°C in a narrow composition range (mole fraction of ZrF_4 = 0.55–0.65) [14]. These values are between −50.5 and −45.4 kJ/mol. Our values, for example −43.3 ± 2.79 kJ/ similar. The ZrF_4–NaF s authors at though the NaF-rich co

Table 2
Enthalpies of transposed-temperature-drop of mechanical mixtures ($\Delta H_{drop}^{mixture}$) from 25 to 900°C for ZN and ZL systems and to 800°C for other systems and enthalpies of mixing of fluorozirconate melts (ΔH_{mix}) in the molten state

Composition of mixtures					$\Delta H_{drop}^{mixture}$ (kJ/mol)	No. of experiments	ΔH_{mix} (kJ/mol)
ZrF_4	BaF_2	LaF_3	AlF_3	NaF			
0.75	0.25				128.72 ± 2.24	3	−22.39 ± 2.23
0.70	0.30				117.10 ± 3.11	3	−30.95 ± 3.08
0.66	0.34				109.70 ± 1.82	4	−35.83 ± 1.82
0.58	0.42				98.12 ± 2.79	3	−43.27 ± 2.79
0.48	0.52				86.03 ± 2.76	4	−49.50 ± 2.77
0.71				0.29	137.54 ± 1.83	3	−10.81 ± 1.72
0.50				0.50	104.83 ± 1.58	3	−23.85 ± 1.64
0.39				0.61	86.85 ± 1.33	2	−31.79 ± 1.45
0.33				0.67	79.73 ± 1.30	3	−33.30 ± 1.34
0.27				0.73	73.65 ± 1.46	2	−33.56 ± 1.99
0.20				0.80	75.21 ± 2.03	3	−25.15 ± 2.06
0.79		0.21			163.31 ± 2.57	3	−1.60 ± 2.59
0.68		0.32			157.66 ± 4.51	3	−1.10 ± 4.80
0.59		0.41			154.00 ± 1.29	3	−0.45 ± 1.35
0.61	0.22			0.17	107.14 ± 2.12	3	−30.11 ± 2.12
0.51	0.26			0.23	88.50 ± 3.00	3	−41.10 ± 3.00
0.55	0.39	0.06			97.16 ± 1.69	3	−42.35 ± 1.69
0.54	0.39		0.07		102.20 ± 1.87	3	−39.62 ± 1.87
0.55	0.37	0.04	0.04		98.94 ± 1.74	3	−42.20 ± 1.74
0.53	0.21	0.04	0.03	0.19	98.12 ± 1.74	3	−35.08 ± 1.74
0.53	0.26	0.03	0.03	0.15	98.33 ± 0.72	3	−36.24 ± 0.72
0.47	0.29	0.03	0.04	0.17	92.92 ± 1.11	3	−38.00 ± 1.11

Error represents two standard deviations of the mean.

Table 3
Enthalpies of t
enthalpies of f

Composition of	
ZrF_4	Ba
0.73	0.2
0.70	0.3
0.66	0.3
0.60	0.4
0.75	
0.63	
0.61	0.2
0.51	0.2
0.55	0.3
0.54	0.3
0.55	0.3
0.53	0.2
0.53	0.2
0.53	0.2
0.47	0.2
0.47	0.2

Error represent
[a] Annealed gla

Table 4
Enthalpies of t
and enthalpies

Crystal
1/3(β-$BaZr_2F$
1/3(α-$BaZr_2F$
1/2(β-$BaZrF_6$)
1/2(α-$BaZrF_6$)
1/3(Ba_2ZrF_8)
1/4(Ba_3ZrF_{10})
1/7($Na_3Zr_4F_1$
1/13(Na_7Zr_6F
1/3(β-Na_2ZrF
1/7(α-Na_5Zr_2
1/4(Na_3ZrF_7)
1/3(meta-LaZr
ZBLAN (0.53–

Error represent

Table 3
Enthalpies of transposed-temperature-drop of glasses (ΔH_{drop}^{glass}) from 25 to 900°C for the ZL system and to 800°C for other systems and enthalpies of formation of fluorozirconate glasses from crystalline fluorides at 25°C (ΔH_{form}^{glass})

Composition of glasses					ΔH_{drop}^{glass} (kJ/mol)	No. of experiments	ΔH_{form}^{glass} (kJ/mol)
ZrF_4	BaF_2	LaF_3	AlF_3	NaF			
0.73	0.27				111.21 ± 1.16	2	12.65 ± 2.88
0.70	0.30				109.37 ± 1.68	2	8.58 ± 3.49
0.66	0.34				104.83 ± 0.20	2	5.21 ± 1.91
0.60	0.40				104.88 ± 0.40	2	−4.41 ± 2.65
0.75		0.25			133.22 ± 2.49	3	28.02 ± 3.22
0.63		0.37			135.59 ± 1.58	3	20.10 ± 3.57
0.61	0.22			0.17	103.66 ± 2.13	3	3.48 ± 3.01
0.51	0.26			0.23	97.02 ± 1.76	2	−8.53 ± 3.48
0.55	0.39	0.06			106.06 ± 1.43	3	−8.90 ± 2.22
0.54	0.39		0.07		106.19 ± 1.08	3	−3.99 ± 2.16
0.55	0.37	0.04	0.04 [a]		105.46 ± 0.89	3	−6.53 ± 1.95
0.53	0.21	0.04	0.03	0.19 [a]	102.02 ± 0.30	3	−3.90 ± 1.77
0.53	0.26	0.03	0.03	0.15	103.25 ± 1.87	3	−4.91 ± 2.01
0.53	0.26	0.03	0.03	0.15 [a]	103.87 ± 0.93	3	−5.54 ± 2.09
0.47	0.29	0.03	0.04	0.17	98.73 ± 0.81	3	−5.82 ± 1.37
0.47	0.29	0.03	0.04	0.17 [a]	100.33 ± 1.40	3	−7.42 ± 1.62

Error represents two standard deviations of the mean.
[a] Annealed glass.

± 2.79 kJ/mol at mole fraction of $ZrF_4 = 0.58$, are similar. The enthalpies of mixing for the molten ZrF_4–NaF system have been investigated by several authors at different temperatures [15–18,28]. Although the minima of enthalpies of mixing are at NaF-rich compositions for each study, their values range from −30 to −43 kJ/mol. Because of the high vapor pressure of ZrF_4, there is considerable uncertainty of the mixing composition range for these high temperature experiments using open systems. Our minimum in heat of mixing, near mole fraction of $ZrF_4 = 0.25$, is −33.6 kJ/mol.

Table 4
Enthalpies of transposed-temperature-drop of crystals ($\Delta H_{drop}^{crystal}$) from 25 to 900°C for ZN and ZL systems and to 800°C for other systems and enthalpies of formation of fluorozirconate crystals from crystalline fluorides at 25°C ($\Delta H_{form}^{crystal}$)

Crystal	$\Delta H_{drop}^{crystal}$ (kJ/mol)	No. of experiments	$\Delta H_{form}^{crystal}$ (kJ/mol)
1/3(β-$BaZr_2F_{10}$)	110.78 ± 3.42	4	0.71 ± 4.06
1/3(α-$BaZr_2F_{10}$)	112.57 ± 2.45	3	−1.07 ± 3.29
1/2(β-$BaZrF_6$)	104.50 ± 0.58	2	−15.91 ± 2.83
1/2(α-$BaZrF_6$)	107.73 ± 2.46	2	−19.15 ± 3.70
1/3(Ba_2ZrF_8)		2	−27.76 ± 2.90
1/4(Ba_3ZrF_{10})		2	−10.53 ± 3.18
1/7($Na_3Zr_4F_{19}$)	116.27 ± 1.68	3	−0.32 ± 2.37
1/13($Na_7Zr_6F_{31}$)	110.00 ± 2.04	3	−11.57 ± 2.53
1/3(β-Na_2ZrF_6)	95.03 ± 0.44	3	−15.14 ± 1.37
1/7(α-$Na_5Zr_2F_{13}$)	88.86 ± 1.58	3	−13.67 ± 2.12
1/4(Na_3ZrF_7)	91.50 ± 0.72	3	−17.43 ± 1.79
1/3(meta-$LaZr_2F_{11}$)	138.01 ± 1.16	5	19.28 ± 4.45
ZBLAN (0.53–0.21–0.04–0.03–0.19)	110.69 ± 1.53	2	−12.57 ± 2.32

Error represents two standard deviations of the mean.

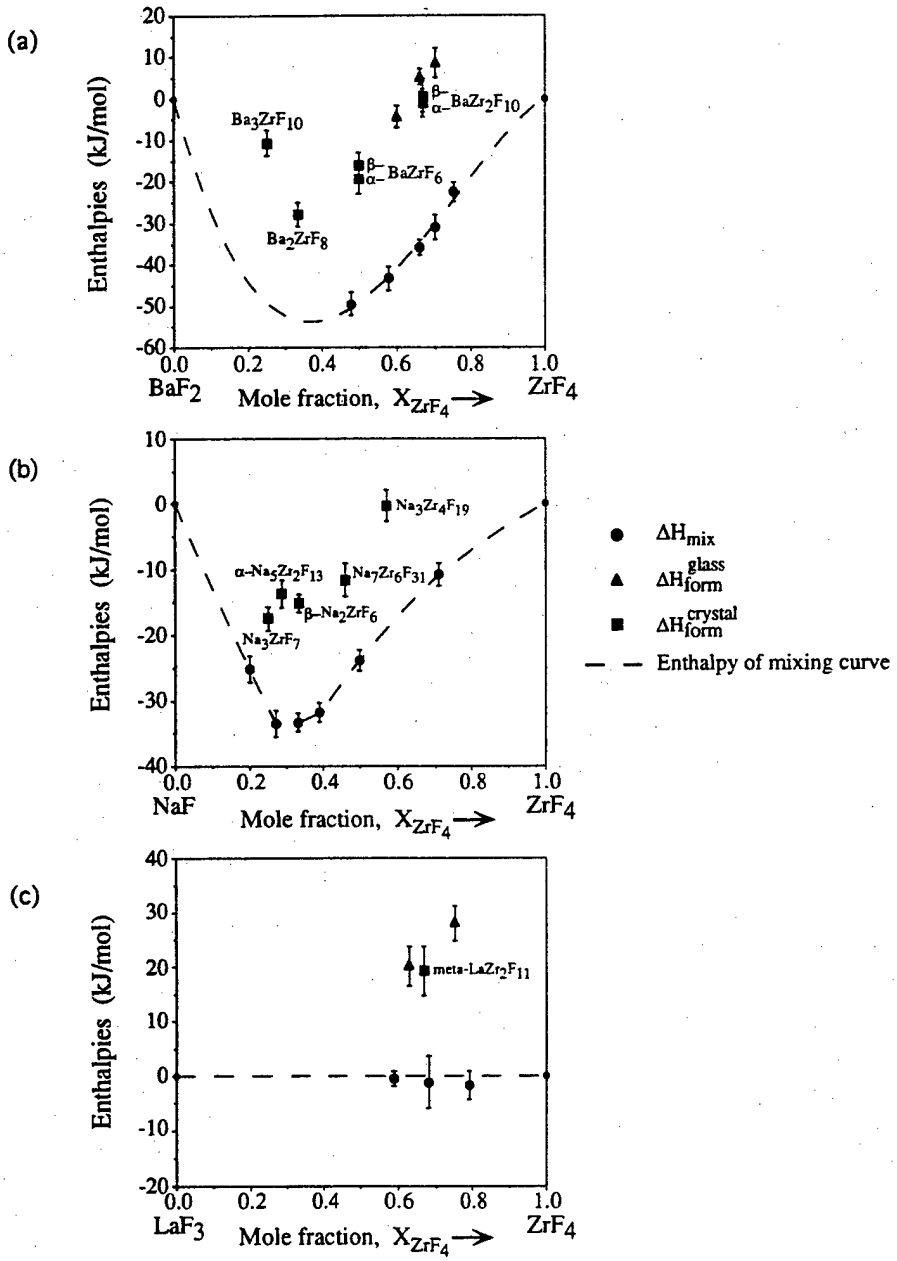

Fig. 1. Enthalpies of mixing of melts (from molten end-members at high temperature), enthalpies of formation of glasses and enthalpies of formation of crystals (from crystalline end-members at 25°C) in binary systems: (a) ZrF_4–BaF_2, (b) ZrF_4–NaF and (c) ZrF_4–LaF_3.

Because we used sealed Au capsules, enthalpy effects related to vaporization, volatile loss, and compositional change were minimal. Several primary observations stand out: (1) The enthalpies of mixing for the molten ZrF_4–BaF_2 and ZrF_4–NaF systems are strongly exothermic. In contrast the system ZrF_4–LaF_3 shows essentially zero heat of mixing in the melt. (2) In the system ZrF_4–BaF_2 the most exother-

Table 5
Enthalpies of vitrification of fluorozirconate glasses at 25°C

Glass	ΔH_{form}^{glass} (kJ/mol)	Corresponding crystals	$\Delta H_{form}^{crystal}$ (kJ/mol)	Heat of vitrification

Table 5
Enthalpies of vitrification of fluorozirconate glasses at 25°C

Glass	ΔH_{form}^{glass} (kJ/mol)	Corresponding crystals	$\Delta H_{form}^{crystal}$ (kJ/mol)	Heat of vitrification (kJ/g atom)
$0.75ZrF_4 \cdot 0.25LaF_3$	28.02 ± 3.22	$0.75[1/3(LaZr_2F_{11})]+0.25ZrF_4$	14.46 ± 3.85	2.85 ± 2.30
$0.63ZrF_4 \cdot 0.37LaF_3$	20.10 ± 3.57	$0.05LaF_3+0.95[1/3(LaZr_2F_{11})]$	18.22 ± 4.33	0.41 ± 2.61
$0.73ZrF_4 \cdot 0.27BaF_2$	12.65 ± 2.88	$0.81[1/3(\beta BaZr_2F_{10})]+0.19\ ZrF_4$	0.58 ± 3.65	2.71 ± 2.20
$0.70ZrF_4 \cdot 0.30BaF_2$	8.58 ± 3.49	$0.90[1/3(\beta BaZr_2F_{10})]+0.10ZrF_4$	0.64 ± 3.85	1.80 + 2.48
$0.66ZrF_4 \cdot 0.34BaF_2$ [a]	5.21 ± 1.91	$0.04[1/3(\beta BaZrF_6)]+0.96[1/3(\beta BaZr_2F_{10})]$	0.05 ± 4.02	1.20 ± 2.14
$0.60ZrF_4 \cdot 0.40BaF_2$	−4.41 ± 2.65	$0.40[1/3(\beta BaZrF_6)]+0.60[1/3(\beta BaZr_2F_{10})]$	−5.94 ± 3.62	0.36 ± 2.19
ZBLAN (0.53–0.21–0.04–0.03–0.19)	−3.90 ± 1.77	ZBLAN (0.53–0.21–0.04–0.03–0.19)	−12.57 ± 2.32	2.20 ± 1.47
$CaMgSi_2O_6$				8.58 [b]
$CaAl_2Si_2O_8$				5.98 [b]
$NaAlSi_3O_8$				3.98 [b]
K_2SiO_3				1.50 [b]

Error represents two standard deviations of the mean.
[a] Enthalpy of fusion of $\beta BaZr_2F_{10}$ = 3.08 kJ/g atom [28].
[b] Data taken from Ref. [43].

mic crystalline compound is Ba_2ZrF_8 at mole fraction of $ZrF_4 = 1/3$. This composition, which is not molten at 800°C, is also near the minimum in the polynomial curve fit to the liquid–liquid heat of mixing data. For the ZrF_4–NaF system, the minimum occurs at a mole fraction of $ZrF_4 = 0.25$ (crystalline phase Na_3ZrF_7) for both crystals and liquids. (3) The enthalpy of formation of the glasses and crystals from crystalline end-members are very similar. They are less exothermic than the enthalpy of mixing in the corresponding melts. In ZrF_4–LaF_3, the crystalline compound (meta-$LaZr_2F_{11}$) and the two glass compositions measured show endothermic heats of formation.

Table 5 shows the enthalpies of vitrification, i.e., the enthalpy differences between glass and corresponding crystals at 25°C and some data for silicates are included for comparison. The enthalpies of vitrification for fluorozirconates are strikingly small, comparable, on a gram-atom basis, to the values for relatively depolymerized silicates e.g. K_2SiO_3 [43]. The enthalpies of formation of annealed glasses are slightly more exothermic than those of normally quenched glasses. This indicates that further structural relaxation occurs and leads to a lower-energy state in annealed glass. However, this effect is relatively small, only 0.1–0.4 kJ/g atom in magnitude.

4. Discussion

4.1. Major complexation reactions

It is clear that the exothermic enthalpies of mixing in the systems ZrF_4–BaF_2 and ZrF_4–NaF are dominated by strong acid–base reactions involving the transfer of fluoride ion to zirconium. In these two binary systems, the enthalpy of mixing of melts and the enthalpy of formation of crystals show minima at the same compositions, Ba_2ZrF_8 and Na_3ZrF_7, respectively, indicating the stoichiometric complexes ZrF_8^{4-} and ZrF_7^{3-}. Crystalline Ba_2ZrF_8 has a structure built of isolated ZrF_8 polyhedra [37], while crystalline Na_3ZrF_7 contains isolated ZrF_7 polyhedra [38]. Indeed, Zr is coordinated by seven or eight fluorine atoms in all solid phases, either crystals or glasses, in related systems [39–41]. Our data are consistent with the energetics being dominated in

melts, glasses and crystals by these same complexes: ZrF_8 and ZrF_7. Although the minimum of enthalpies of mixing in ZrF_4–BaF_2 could not be measured directly at 800°C due to its higher melting temperature, such consistency in energetics may indicate that the enthalpy of mixing behavior is effectively independent of temperature. This is intimately associated with the mixing mechanism in melts, which will be discussed in the next section. The smaller coordination number for the molten ZrF_4–NaF system may reflect the need of smaller countercations to mix with the smaller anionic complexes for proper geometrical packing in the melt.

For the reaction

$$2BaF_2 + ZrF_4 = Ba_2ZrF_8$$

the enthalpy is about -160 kJ/mol in the melts at 800°C and -83 kJ/mol for crystals at 25°C. For the reaction

$$3NaF + ZrF_4 = Na_3ZrF_7$$

the enthalpy is about -134 kJ/mol in the melts at 900°C and -52 kJ/mol for crystals at 25°C. The enthalpy of formation in the solid state (crystals from crystalline end-members) is less exothermic than that in the molten state (melts from molten end-members). The large heat of fusion of ZrF_4 is mainly responsible for this difference. Since crystalline ZrF_4 consists of corner-shared ZrF_8 polyhedra, the large heat of fusion represents mainly the depolymerization of such polyhedra. We will use these observations below to argue that ZrF_4-rich melts, including molten ZrF_4 itself, contain Zr in lower coordination.

Enthalpies of mixing in ZrF_4–LaF_3 melts are essentially zero. This implies that no strong complexes are formed in this system. This is seen also in the positive heats of formation of the crystalline compound meta-$LaZr_2F_{11}$. Although its structure is not known in detail, it probably contains considerable disorder and is apparently stabilized by entropy rather than enthalpy. LaF_3 is a Lewis acid which forms complexes in the same way as ZrF_4. Thus there can be no strong acid–base reactions between them. Molten lanthanum fluoride-alkali fluoride mixtures do show somewhat exothermic heats of mixing at 1087°C, although Hong and Kleppa did not suggest that LaF_3 is a complex former [42].

The barium fluorozirconate crystals are Ba_2ZrF_8 with isolated ZrF_8 polyhedra [37], β-$BaZrF_6$ with chains of edge-sharing ZrF_8 polyhedra [40] and β-$BaZr_2F_{10}$ with layers of ZrF_7 units [30]. The amount of Ba participating in the structures decreases in that order, as does the amount of ionic bonding. The enthalpy of formation becomes less exothermic in this series, showing that the ionic interaction of fluorozirconate polyhedra and countercations contributes to the stability of the crystal. This trend is expected in ZrF_4–NaF, as enthalpies of formation of crystals also become less exothermic toward ZrF_4-rich compositions.

The solid–liquid phase diagrams for three binary systems have been studied by Grande et al. [26–28]. The binary systems ZrF_4–BaF_2 and ZrF_4–NaF with strongly negative enthalpies of mixing form several crystalline compounds. We have noted that the melts have even more strongly negative heats of mixing than the heats of formation of these crystals and this stabilization of the melts is present over a continuously varying composition range. The result is that the free energy of mixing in the melts must deviate strongly from ideality (whatever the details of entropy of mixing) and this deviation is more pronounced in the molten state than that in the solid state. The consequence is a significant lowering of the free energy of the molten state relative to the mixture of crystals which would form at intermediate compositions, a steep depression of freezing point curves and the creation of deep eutectics between the solid-state compounds, as seen in the experimental phase diagrams ZrF_4–BaF_2 and ZrF_4–NaF. In contrast, the system ZrF_4–LaF_3, without strong complexation, behaves more nearly as an ideal solution and shows a much gentler freezing point depression.

4.2. A structural model for fluorozirconate melts

ZrF_4-rich compositions have less fluoride ions, dissociated from alkali and alkaline earth fluorides, available to form ZrF_8^{4-} or ZrF_7^{3-}. Data in the literature suggest that anionic complexes would be coordinated by fewer fluoride ions. First, in Raman spectroscopic studies of fluorozirconate melts by Toth and Boyd [20,21], several crystalline compounds with different coordination number of F about Zr were also investigated. They found that the occurrence of anionic complexes can be inferred from frequency

shifts and concluded that the coordination number of F about Zr decreases from 8 to 5 or 4 with increasing ZrF_4 content. Second, the viscosities decrease from the composition $0.5BaF_2 \cdot 0.5ZrF_4$ to the composition $1/3BaF_2 \cdot 2/3ZrF_4$ in the binary system ZrF_4–BaF_2 [12], which can be rationalized if the size of anionic complexes is considered as an important factor controlling the mobility. Third, since a decrease in coordination number of anionic complexes towards the ZrF_4-rich compositions would be expected to lead to a less exothermic heat of mixing, our calorimetric data also support this argument.

Zirconium is eight-coordinated by fluorine in solid ZrF_4 and a considerably lower coordination number in the molten state would be in agreement with the large entropy of fusion and the large enthalpy of fusion [28]. It would also be consistent with the less exothermic enthalpies of formation of crystals than of melts as discussed above. This is further supported by the smaller heat capacities of melts relate to crystals [33] because of the likely increase of the Zr–F bond strength with lower coordination number. Thus we propose ZrF_4 as the low coordination number entity in the molten state for pure ZrF_4. This then provides a simple model for molten binary fluorozirconates at high temperature. For the system ZrF_4–BaF_2, anionic complexes can be formed between ZrF_4 and F^- and their average coordination number decreases from 8 to 4 with increasing ZrF_4 content. The system ZrF_4–NaF shows a similar trend, but the maximum coordination number of F about Zr for an anionic complex is 7. It will be helpful to use the following examples to describe this model. In the system ZrF_4–BaF_2, $1/3BaF_2 \cdot 2/3ZrF_4$ is the best composition for glass formation and its speciation is

$$1/3(Ba^{2+} + 2F^-) + 2/3ZrF_4 \rightarrow 1/3Ba^{2+} + 2/3ZrF_5^- .$$

Speciation for the composition $0.25BaF_2 \cdot 0.75ZrF_4$ with less F^- available is

$$0.25(Ba^{2+} + 2F^-) + 0.75ZrF_4 \rightarrow 0.25Ba^{2+} + 0.5ZrF_5^- + 0.25ZrF_4 .$$

Similarly, the reaction for mixing 0.5NaF with $0.5ZrF_4$ is

$$0.5(Na^+ + F^-) + 0.5ZrF_4 \rightarrow 0.5Na^+ + 0.5ZrF_5^- .$$

The last two reactions have $0.5ZrF_5^-$ formed and have the same net reactions:

$$0.5F^- + 0.5ZrF_4 \rightarrow 0.5ZrF_5^- .$$

From our measurements, the enthalpies of mixing for these two reactions are very similar (see Table 2). This supports the usefulness of this structural model for molten fluorozirconates and suggests that formation of anionic complexes is the dominant exothermic contribution. Other factors may influence the mixing mechanism and thermodynamic properties of those melts, such as the interactions between anionic complexes and countercations or the competition between ZrF_4 for limited F^-. However, when adding more BaF_2 or NaF, ZrF_4 will be more highly coordinated by F^- and Zr–F bond formation in anionic complexes will dominate the energetics.

The ideas above concerning complex formation and speciation can be extended to multicomponent fluorozirconate melts. Enthalpies of mixing of molten binary mixtures of AlF_3 with alkali fluorides were found to be exothermic and the result was interpreted in terms of complex formation [44]. Therefore, we assume that ZrF_4, LaF_3 and AlF_3 are anionic complex formers. They do not contribute fluoride ions to raise the coordination number of Zr and their mixing energetics with each other are not strongly exothermic. BaF_2, NaF and other alkali and alkaline earth fluorides are fully ionized in the melt. Their free fluoride ions become coordinated to the anionic complex formers. Their enthalpies of mixing with ZrF_4 are strongly exothermic. We then define the average coordination number of Zr, N, as four plus the number of free fluoride ions available per anionic complex former. For example, for the composition $1/3BaF_2 \cdot 2/3ZrF_4$, which is the best glass-forming composition in that binary system, $N = 4 + (1/3 \times 2)/(2/3) = 5$ and Zr would have an average coordination number of five. The ZBLAN20 multicomponent glass [11], the best glass-former found so far has the composition $0.53ZrF_4$–$0.20BaF_2$–$0.04LaF_3$–$0.03AlF_3$–$0.20NaF$. It has $N = 4 + ((0.20 \times 2) + 0.20)/(0.53 + 0.04 + 0.01) = 5$. This again corresponds to an average of five fluorines around Zr. For the non-glass-forming composition Ba_2ZrF_8, $N = 4 + (2 \times 2)/1 = 8$ and for Na_3ZrF_7, $N = 4 + 3/1 = 7$, in accord with the expected complexation in these melts.

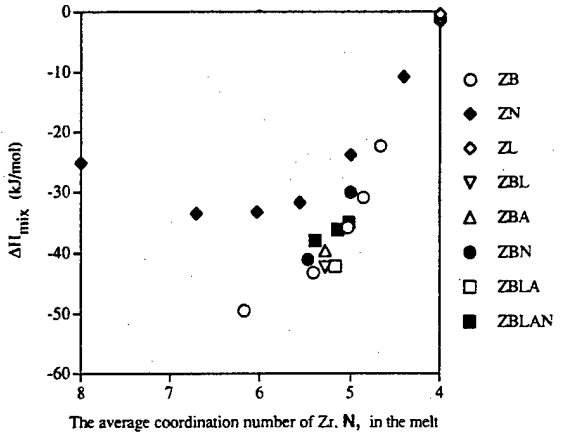

Fig. 2. Enthalpy of mixing of melts (from molten end-members at high temperature) versus the average coordination number of Zr, N, in the melt.

Fig. 2 shows the enthalpy of mixing of binary and multicomponent melts as a function of the average coordination number of Zr, N, calculated as defined above. The enthalpy of mixing becomes more exothermic with increasing average coordination number of Zr. The generally smooth trend for all systems suggests that the complex-forming reaction dominates the energetics. With the same average coordination numbers, substituting NaF for BaF_2 mainly implies that a smaller amount of anionic complexes are formed in melts, reflecting the less exothermic effects. However, we do not have enough data to investigate further the differences between cations or the relative affinities of Zr, La and Al for fluoride ion in a systematic fashion.

4.3. Thermodynamic factors affecting glass formation

Fig. 3 shows the enthalpy of formation of glasses from crystalline fluorides at 25°C versus N, the average coordination of Zr in the melt, as defined above. It is noteworthy that, in multicomponent as well as simple systems, the glass-forming compositions are concentrated between $N = 4.5$ and 5.5. A search through the literature also confirms that the vast majority of glass-forming compositions in ZrF_4-based systems fall in the range on $N = 5.0 \pm 0.5$ (One exception is $BaZrF_6$ glass prepared by quenching the melt rapidly using a twin roller [24].) In addition, glass formation appears more favorable near $N = 5.0$ and the empirically derived good glass-forming compositions appear to be those which can maximize the concentration of ZrF_5^- species. These compositions all lie in the region dominated by deep eutectics in both binary and multicomponent systems. It suggests that the melt near $N = 5.0$ is thermodynamically more stable than its corresponding crystals over a wide temperature interval, and results in a deep eutectic. The presence of ZrF_5^- in melts has been verified by several spectroscopic studies [20–22].

From most structural studies of glasses [5–8], zirconium in the glassy state is coordinated by 7 or 8 fluorine atoms through sharing some of them. Our data have also shown that ZrF_7 and ZrF_8 are energetically favorable species. Thus, the glass-forming melt must undergo considerable restructuring as it cools to and through the glass transition. However, the binary system ZrF_4–NaF is not glass-forming even near $N = 5.0$ where it has a deep eutectic. This implies that glass formation must also be contributed by kinetic factors. If nucleation and crystallization require fluctuations extending over distances somewhat greater than those involved in structural relaxation for glass formation [13], the relatively expected low viscosity of the melt near $N = 5.0$ at deep eutectics in the system ZrF_4–NaF may be a factor. In other words, glass-forming ability is initiated by the

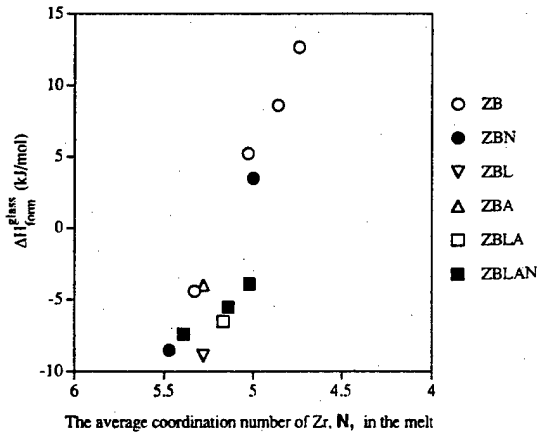

Fig. 3. Enthalpy of formation of glasses from crystalline fluorides at 25°C versus the average coordination number of Zr, N, in the melt.

formation of ZrF_5^- and is further supported by the kinetic factors (e.g. viscosity) in melts.

What, then, is the role of the minor additives, LaF_3 and AlF_3, in further enhancing glass formation? The arguments above and correlations in Figs. 2 and 3 suggest that energetic stabilization by La and Al is not a factor. Rather, these complex anions add to the heterogeneity and diversity of local structures in the melt and they may exert a kinetic role hindering nucleation. This general observation, namely the glasses form more easily in complex systems, is sometimes called the 'confusion principle' [2], but it is hard to express quantitatively. The system ZrF_4–LaF_3 does form some glasses, under rapid quench conditions. Because no stable anionic complexes are formed in this system, the reason for glass formation must be different from those in the rest of the ZBLAN system. As the melt cools into the vitreous state, ZrF_4 species and LaF_3 species must both be incorporated into the glassy structure, probably with an increase in coordination number resulting from linkages of adjacent polyhedra. However, structural details are not known.

We conclude that the following factors favor glass formation in fluorozirconate systems: (a) the thermodynamic factors near deep eutectics: formation of stable anionic complexes, e.g. ZrF_5^-, in the melts which leads to deep eutectics and major structural changes in the melt on cooling and (b) the confusion principle: increasing structural diversity in the melt by adding small amounts of other components, NaF, LaF_3 and AlF_3, without significantly changing the value of $N = 5.0$.

The small enthalpy difference between glass and crystal (small enthalpy of vitrification) implies some similarity in structures, as seen in a similar trend of increasing exothermicity with increasing N (i.e., increasing alkali or alkaline earth fluoride content) in glass and crystal (see Figs. 1 and 3). It also implies only a small thermodynamic driving force for crystallization of the glass once it is near or below the glass transition. Although these traditional considerations relating crystallization or nucleation are significant, we now propose that the thermodynamic factors related to the restructuring are also very important for glass formation in fragile liquids. Further experimental approaches to this subject are proceeding.

5. Conclusion

This study provides improved measurements of enthalpies of mixing of fluorozirconate melts by transposed-temperature-drop calorimetry of samples in sealed Au-capsules. Enthalpies of formation of glasses and crystals have been investigated for the first time. A structural model is proposed in which glass-forming melts are dominated by ZrF_5^- species. In contrast to the similarity of structures between supercooled liquids and glasses near the glass transition, there are significant differences in structure between melts at high temperature and glasses. Therefore, as temperature decreases below the liquidus, a substantial structural change must occur. Such restructuring with temperature of a fragile liquid appears intimately linked to glass-forming ability in fluorozirconate systems.

Acknowledgements

This work was supported by the National Science Foundation (Grant DMR 92-15802) and New Jersey State Commission on Science and Technology and the Fiber Optic Material Research Program.

References

[1] M. Poulain, J. Non-Cryst. Solids 184 (1995) 103.
[2] C.T. Moynihan, Mater. Res. Soc. Bull. 15 (1987) 40.
[3] J.M. Parker, P.W. France, in: Glass and Glass-Ceramics, ed. M.H. Lewis (Chapman and Hall, 1989) p. 156.
[4] A.E. Comyns, ed., Fluoride Glasses (Wiley, New York, 1989).
[5] J. Lucas, Mater. Sci. Forum 19&20 (1987) 3.
[6] A.P. Kulikov, V.K. Goncharuk, T.I. Usoltseva, G.S. Yuriev, Nucl. Instrum. Methods Phys. Res. 282 (1989) 583.
[7] C.C. Phifer, D.J. Gosztola, J. Kieffer, C.A. Angell, J. Chem. Phys. 94 (1991) 3440.
[8] J.H. Simmons, G. O'Rear, T.P. Swiler, A.C. Wright, J. Non-Cryst. Solids 106 (1988) 325.
[9] H. Hu, J.D. Mackenzie, J. Non-Cryst. Solids 54 (1983) 241.
[10] K. Matusita, M. Koide, T. Komatsu, J. Non-Cryst. Solids 140 (1992) 119.
[11] W.C. Hasz, C.T. Moynihan, J. Non-Cryst. Solids 140 (1992) 285.
[12] T. Grande, H.A. Oye, S. Julsrud, J. Non-Cryst. Solids 161 (1993) 152.
[13] C.A. Angell, J. Non-Cryst. Solids 73 (1985) 1.

[14] G. Hatem, K. Mahmoud, M. Gaune-Escard, Thermochim. Acta 182 (1991) 91.
[15] A. Fontana, R. Winand, J. Nucl. Mater. 44 (1972) 305.
[16] G. Hatem, F. Tabaries, M. Gaune-Escard, Thermochim. Acta 149 (1989) 15.
[17] T. Grande, S. Julsrud, Mater. Sci. Forum 32&33 (1988) 643.
[18] M. Gaune-Escard, G. Hatem, P. Gaune, M. Hoch, Mater. Sci. Forum 67&68 (1991) 285.
[19] J.K. Wilmshurst, J. Chem. Phys. 39 (1963) 2545.
[20] L.M. Toth, A.S. Quist, G.E. Boyd, J. Phys. Chem. 77 (1973) 1384.
[21] L.M. Toth, G.E. Boyd, J. Phys. Chem. 77 (1973) 2654.
[22] G.E. Walrafen, M.S. Hokmabadi, S. Guha, P.N. Krishnan, D.C. Tran, J. Chem. Phys. 83 (1985) 4427.
[23] A.A. Babitsyna, T.A. Emel'yanova, A.P. Chernov, Russ. J. Inorg. Chem. 34 (1989) 1798.
[24] Y. Kawamoto, F. Sakaguchi, Bull. Chem. Soc. Jpn. 56 (1983) 2138.
[25] C.J. Barton, W.R. Grimes, J. Insley, R.E. Moore, R.E. Thoms, J. Phys. Chem. 62 (1958) 665.
[26] S. Aasland, T. Grande, S. Julsrud, J. Non-Cryst. Solids 140 (1992) 69.
[27] T. Grande, S. Aasland, S. Julsrud, J. Non-Cryst. Solids 140 (1992) 73.
[28] T. Grande, PhD thesis, University of Trondheim (1992).
[29] C.C. Phifer, C.A. Angell, J.P. Laval, J. Lucas, J. Non-Cryst. Solids 94 (1987) 315.
[30] J.P. Laval, B. Frit, J. Lucas, J. Solid State Chem. 72 (1988) 181.
[31] A. Navrotsky, Mater. Res. Soc. Symp. Proc. 321 (1994) 3.
[32] L. Topor, A. Navrotsky, in: Application to Earth and Planetary Sciences, High-Pressure Research, ed. Y. Syono and M.H. Manghnani (1992) p. 71.
[33] L.B. Pankratz, ed., Thermodynamic Properties of Halides, U.S. Bur. Mines. Bull. vol. 674, 1984.
[34] R.A. McDonald, G.C. Sinke, D.R. Stull, J. Chem. Eng. Data 7 (1962) 83.
[35] JANAF Thermochemical Tables, 1985.
[36] L. Topor, A. Navrotsky, Y. Zhao, D.J. Weidner, EOS Trans. Am. Geophys. Union 73 (1992) 300.
[37] J.P. Laval, B. Frit, Acta Crystallogr. B36 (1980) 2533.
[38] L.A. Harris, Acta Crystallogr. 12 (1959) 172.
[39] J.P. Laval, B. Frit, Acta Crystallogr. B34 (1978) 1070.
[40] B. Mehlhorn, R. Hoppe, Z. Anorg. Allg. Chem. 425 (1976) 180.
[41] J.H. Burns, R.D. Ellison, H.A. Levy, Acta Crystallogr. B24 (1968) 230.
[42] K.C. Hong, O.J. Kleppa, J. Phys. Chem. 83 (1979) 2589.
[43] A. Navrotsky, Physics and Chemistry of Earth Materials (Cambridge, 1994) p. 382.
[44] K.C. Hong, O.J. Kleppa, J. Phys. Chem. 82 (1978) 176.

N·H
ELSEVIER

Abstract

Heat capa
(DSC) and t
capacities of
between the g
supercooled l
conate exhib
restructuring
structural cha
allows the su
resulting in a
controlled by

PACS: 05.70.-a

1. Introduc

Heavy m
rozirconate
15 years be
cations [1–4
binary syste
of glass forr
nent fluorid
AlF_3–NaF)
devitrificatic

* Correspond
258 1274; e-ma

0022-3093/97/
PII S0022-3(

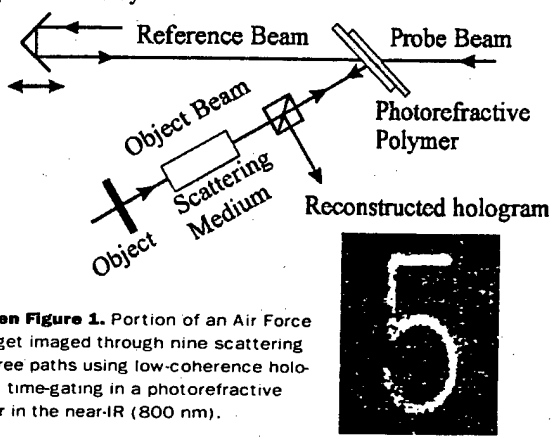

Kippelen Figure 1. Portion of an Air Force bar-target imaged through nine scattering mean free paths using low-coherence holographic time-gating in a photorefractive polymer in the near-IR (800 nm).

beam. The light can be provided either by a short-pulse or low-coherence laser source such as a superluminescent laser diode. Filtering is achieved by adjusting the relative time delay between the object and the reference beams. The information carried by the ballistic light is then reconstructed by reading out the recorded hologram in a four-wave mixing geometry.

A key enabler for imaging of biological tissues using HTG, is the availability of a real-time optical recording material with high resolution and high sensitivity in the near-IR spectrum, where biological tissues have a good transparency (700–900 nm). Due to their high efficiency and ability to be easily processed into large area films at low cost, photorefractive polymers offer a lot of potential. Recently, by using (2, 4, 7-trinitro-9-fluorenylidene) malonitrile (TNFDM) as a sensitizer, we were able to extend the spectral sensitivity of previous materials (633–690 nm) to the near-IR (830 nm).[4, 5] Polymer composites of DHADC-MPN:PVK: ECZ:TNFDM with a diffraction efficiency of $\eta = 74\%$ at a field of $E = 59$ V/μm at 830 nm, were developed, and imaging by HTG using a Ti:Sapphire laser in either the pulsed or cw regime was demonstrated (see Fig. 1).

Polymers as recording materials offer a number of advantages over recording media used previously in the near-IR: They are faster and more efficient than $BaTiO_3$ crystals[2] and they have a higher resolution than photorefractive semiconductor multi-quantum wells.[3] Compared to other imaging techniques, this method potentially offers a fast acquisition time since no scanning, computation, or digital processing is involved. The manufacturing cost of such a system is low, because it uses a highly efficient photorefractive polymer with low cost as recording material that is compatible with superluminescent low-coherence laser diodes. This imaging technique, therefore, could become a valuable new medical diagnosis tool.

Acknowledgments

The authors acknowledge collaboration with Eric Hendrickx, Harald Röckel, Boris Volodin, and Derek Steele. This work was supported by AFOSR, NSF, and ONR through the MURI program CAMP.

References

1. S.K. Gayen and R.R. Alfano, "Emerging optical biomedical imaging techniques," Opt. & Phot. News **7** (3), 16 (1996).
2. S.C.W. Hyde *et al.*, "Depth-resolved holographic imaging through scattering media by photorefraction," Opt. Lett. **20**, 1331 (1995).
3. R. Jones *et al.*, "Direct-to-video holographic readout in quantum wells for three-dimensional imaging through turbid media," Opt. Lett. **23**, 103 (1998).
4. B. Kippelen *et al.*, "Infrared photorefractive polymers and their applications for imaging," Science **279**, 54 (1998).
5. D.D. Steele *et al.*, "Transillumination imaging through scattering media by use of photorefractive polymers," Opt. Lett. **23**, 153 (1998).

COMMUNICATIONS

Highly Efficient 1.3-μm Luminescence from Rare-earth-doped Halides Prepared from Low Temperature Aqueous Solutions

John Ballato, Richard E. Riman, and Elias Snitzer, Dept. of Ceramic & Materials Engineering, Rutgers Univ., Piscataway, NJ.

The tremendous growth in photonic materials and device research results largely from the explosion in telecommunications, including the traffic requirements needed for the Internet and future interactive video and multimedia services. These trends have motivated a global search for materials suitable for optical amplification at the 1.3-μm zero dispersion wavelength, which maximizes the information carrying capacity of silica fibers. Praseodymium (Pr^{3+}) has received the most attention as a dopant for gain at 1.3 μm and has reached some level of commercialization[1] despite a relatively low quantum yield from the requisite nonoxide glass hosts (~10 %). Dysprosium (Dy^{3+}) has also attracted recent interest since its absorption cross-section is larger than Pr^{3+} thus lessening the requisite amplifier length.[2] In both cases, maximizing the luminescence efficiency requires hosts with low phonon energies. Accordingly, we considered the solution-synthesis of doped-lanthanum halides because of their low phonon energy and high rare-earth solubility.[3,4]

Lanthanum halides are prepared by dissolving hydrated $LaCl_3$ (and $PrCl_3$ or $DyCl_3$) in deionized water, precipitating $La(OH)_3$ from a solution using NH_4OH, and reactive atmosphere processing in an alumina muffle-tube furnace with an anhydrous halogenating gas (*i.e.*, hydrogen fluoride or hydrogen chloride). Compositions and phases are validated using X-ray diffraction and combustion analyses. Fluorescence at 1.3 μm was observed for the first time from aqueous solution-derived materials. Luminescence from 750 ppm Pr^{3+}-doped LaF_3 samples, HF treated at 600°C, decayed with a 0.23-ms lifetime and a radiative efficiency of 8%, as calculated from Judd-Ofelt analysis.[4, 5] The emission possessed a 3-dB bandwidth of approximately 100 nm (1280 → 1380 nm) making it of interest for WDM systems. Luminescence at 1.3 μm from a 500 ppm Pr^{3+}-doped $LaCl_3$ sample was also equally broad-band (1290 → 1400 nm) with lifetimes for the 200°C chlorinated samples on the order of 1 ms, with a slight increase to 1.3 ms if chlorination occurs at 400°C. Radiative

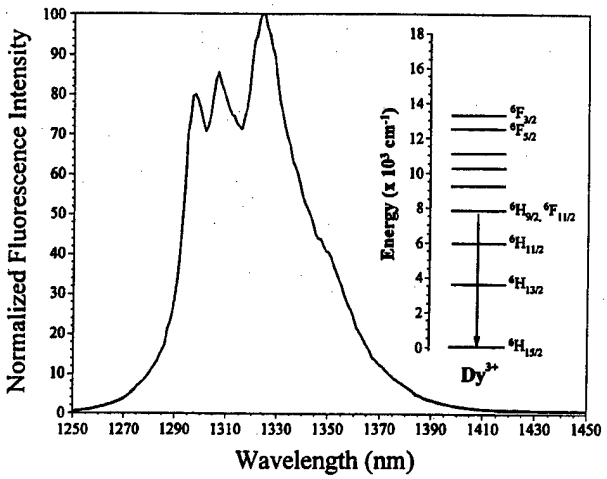

Ballato Figure 1. Normalized fluorescence spectra for solution-derived Dy^{3+}:$LaCl_3$.

efficiencies of 66% and 72% are measured, respectively, for these samples. Dy^{3+}:$LaCl_3$ (500 ppm) samples exhibited relatively narrow 3-dB emission bandwidths of 50 nm (1295 → 1345 nm) (See Fig. 1). Measured lifetimes of 1.11 ms (200°C) and 1.31 ms (400°C) correspond to measured efficiencies of 66% and 78%, respectively.

The spectroscopic properties of these hosts are comparable, if not better, than melt-grown, ultra-pure single-crystal analogs verifying the ability of inexpensive and low-temperature solution-based methodologies to produce low phonon-energy materials. The versatility, ease, and low cost of this solution process represents a significant advance in 1.3 μm fluorescent materials for both optical fiber and thin-film amplifiers for planar integrated photonics.

References

1. T.J. Whitley, "A review of recent system demonstrations incorporating 1.3 μm praseodymium-doped fluoride fiber amplifiers," J. Lightwave Technol. **13,** 744–760 (1995).
2. K. Wei *et al.*, "Spectroscopy of Dy^{3+} in Ge-Ga-S glass and its suitability for 1.3 μm fiber optical amplifier applications," Opt. Lett. **19,** 904–906 (1994).
3. J. Ballato *et al.*, "Sol-gel synthesis of rare-earth-doped lanthanum halides for highly efficient 1.3 μm optical amplification," Opt. Lett. **22,** 691–693 (1997); J. Ballato, "Sol-gel synthesis of rare-earth-doped halide optical materials for photonic applications," Ph.D. Thesis, Dept. of Ceramic & Materials Engineering, Rutgers Univ., Piscataway, NJ (1997).
4. M.J. Weber, "Spontaneous emission probabilities and quantum efficiencies for excited states of Pr^{3+} in LaF_3," J. Chem. Phys. **48,** 4774–4780 (1968); L.B. Shaw *et al.*, "Radiative and multiphonon relaxation of the mid-IR transitions of Pr^{3+} in $LaCl_3$," IEEE J. Quantum Electron. **32,** 2166–2172 (1996).
5. R.H. Page, *et al.*, "Dy-doped chlorides as gain media for 1.3 μm telecommunications amplifiers," J. Lightwave Technol. **15,** 786–793 (1997).

High-speed Multi-wavelength Photonic Switch

N.A. Riza, CREOL and The School of Optics, Univ. of Central Florida, Orlando, FL.

The ability to rapidly and independently switch multiple wavelengths in a light beam is useful for both WDM fiber-optic communications and for hardware compressed photonic signal processing. Key features for such a multi-wavelength switch include microsecond domain wavelength switching and excellent –50 dB optical switching isolation, leading to rapidly reconfigured high signal-to-noise ratio photonic systems. Previously, the bulk acousto-optic tunable filter (AOTF) was found to be attractive for this multi-wavelength switch application as the bulk AOTF can operate over wide optical bandwidths with high speeds and at high optical power levels. Recent improvements in AOTF device designs have lowered the high drive power requirements commonly associated with bulk AOTFs.[1] In addition, these new devices show spectral resolutions in the 1-nm level range, indicating possible use for high (> 32) channel count WDM fiber communications. Nevertheless, one debilitating problem associated with the inherent operation of the AOTF is its finite (*e.g.*, 95%) diffraction efficiency that leads to its low and undesirable –20 dB level type optical crosstalk numbers.

Recently, we proposed a dual-AOTF based multi-wavelength switch structure that solves this inherent AOTF caused low crosstalk problem, hence making it possible to use bulk-AOTF devices for a broad range of multi-wavelength photonic signal processing applications. Specifically, a new high-speed and ultra-high crosstalk suppression multi-wavelength add-drop optical filter structure (see Fig. 1) is demonstrated using two bulk AOTFs.[2] Using simple spatial blocks, polarization optics, and orthogonal set drive conditions for the AOTFs, an average –47 dB optical suppression is measured for the unwanted wavelengths at the filter output ports. The filter is tested for the three standard red, green, and blue visible wavelengths, and demonstrates a switching time of 0.65 μs and an average optical loss of 5 dB. Polarization diversity techniques can be applied to make the switch in Figure 1 insensitive to the input polarization, such as required in fiber-based applications. Applications for this switch can range over a wide optical spectrum, with optimized designs possible for both

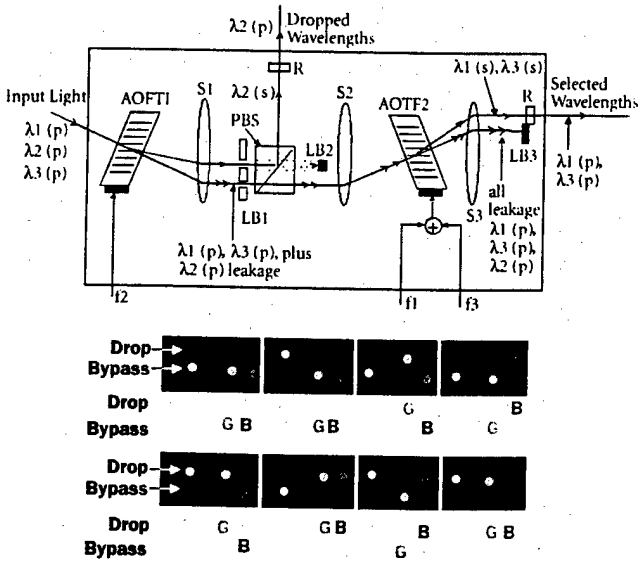

Riza Figure 1. The proposed suppressed crosstalk multi-wavelength filter/switch architecture shown as a drop filter in a 1 × 2 switch configuration for polarized inputs. R = 90° polarization rotator. Figure also shows the drop and bypass port images captured using a video camera. The images show the three independent R, G, B colors as they are switched to the two ports in our experimental filter.

2:00 PM - 2:20 PM (G-025-97)

SILVER INTERDIFFUSION INTO GLASSES CONTAINING ALKALI

E. A. Bolden*; VT FEORC, Washington, DC 20375, (202) 767-9574;
J.E. Shelby, Alfred University, Alfred, NY 14802, (607) 871-2470

The kinetics of the interdiffusion of silver and alkali ions were studied with respect to the type of alkali present, glass composition, and the temperature of heat treatment. Results for the binary glasses suggest that the sodium-silver pair optimizes interdiffusion, although the results for the glasses containing Li^+ were inconclusive due to phase separation. In the glasses that contain a high percentage of K^+, the silver spontaneously reduces to form silver colloids. The rate of exchange increases with Na^+ content of the glass. Increasing heat treatment temperature increases the rate of silver-alkali interdiffusion. The ternary alkali gallosilicate glasses showed that the rate of exchange did increase with increasing alkali content, but the absorbance due to the silver colloids was not as high as the binary silicate glasses. The commercial glasses with high alkali content exchanged readily with the silver. The presence of phase separation in some of the commercial glasses affects the exchange of the silver for the alkali. The rate of exchange increases for the commercial glasses as time and temperature increase.

2:20 PM - 2:40 PM (G-026-97)

BLUE UPCONVERSION CHARACTERISTICS OF THULIUM-DOPED SILICA FIBER WITH HIGH GERMANIA CONTENT

S. Tanabe*, J.D. Prohaska, B. Cole, E. Snitzer, Fiber Optic Materials Research Program, Department of Ceramics, Rutgers University, Piscataway, NJ 08855-0909, *now Faculty of Integrated Studies, Kyoto University, Kyoto 606-01, Japan +81(75)753-6821, tanabe@cheml.kyoto-u.ac.jp

Blue upconversion characteristics of Tm-doped silica fiber with high GeO_2 content and a large NA were investigated by pumping with a tunable DCM-dye laser. Strong blue luminescences at 455nm and 480nm were observed, which are due to the $^1D_2$-$^3F_4$ and $^1G_4$-$^3H_6$ transitions, respectively. The excitation spectra and the pumping power dependences of the intensity for both emissions showed different features. Moreover, these spectroscopic properties changed with changing fiber length from 6m to 0.3m. The peak wavelength of $^1G_4$ emission at the fiber ends also shifted with fiber lengths. These spectroscopic results were explained in terms of the different excited state absorption mechanisms and their competing processes for these two-step upconversions.

2:40 PM - 3:00 PM (G-027-97)

1.3¥im EMISSION AND MULTIPHONON RELAXATION PHENOMENA IN PbO-Bi2O3-Ga2O3 GLASSES DOPED WITH RARE-EARTHS

Yong Gyu Choi, You Song Kim and Jong Heo*, Pohang University of Science and Technology, Pohang, Republic of Korea, +82-562-279-2147

Emissions of 1.3¥im flourescence from PbO-Bi2O3-Ga2O3 glasses doped with Pr3+ and Dy3+ were evaluated. Modified Judd-Ofelt analysis was applied to the Pr3+ -doped glasses in order to obtain more physically meaningful intensity parameters and radiative characteristics. Emission from the Pr3+ : 1G4 --> 3H5 transition in the glass was centered at the wavelength of 1320 nm. Lifetime of the Pr3+ : 1G4 level was 53¥isec with the quantum efficiency of 9%. Excited-state absorption near the 1.3¥im emission were comparable to those in fluoride glasses. Multiphonon relaxation rates of PbO-Bi2O3-Ga2O3 glasses calculated from the lifetimes were similar to those of fluoride glasses but were the lowest among oxide glasses.

3:00 PM - 3:20 PM (G-028-97)

Luminescent Behavior of Sol-Gel-Derived Pr^{3+} and Dy^{3+} doped Lanthanum Halides for 1.3 μm Optical Amplification

John Ballato,* Richard E. Riman, and Elias Snitzer
Rutgers, The State University of New Jersey, *Fiber Optic Materials Research Program*, Brett and Bowser Roads, Piscataway, NJ 08855-0909

Praseodymium- and dysprosium-doped lanthanum halide powders were synthesized via a sol-gel/reactive atmosphere approach and their luminescent properties investigated experimentally and theoretically. Emission at 1.3 μm was observed for the first time from a sol-gel-derived material. Radiative lifetimes on the order of 0.23 msec for a 750 ppm Pr^{3+}:LaF_3 and greater than 1 msec for 500 ppm samples of Pr^{3+} and Dy^{3+}:$LaCl_3$ were measured corresponding to quantum efficiencies of approximately 8 % for Pr^{3+}:LaF_3, 34 % for Pr^{3+}:$LaCl_3$, and 78 % Dy^{3+}:$LaCl_3$. This latter value among the highest quantum efficiency for any halide optical material measured to date. The spectroscopic properties of these aqueously-processed, low-phonon energy hosts are shown to be comparable, or superior to conventionally-prepared, single-crystal analogs. Strategies are discussed to minimize concerns over hydroscopicity and potentially realize highly efficient planar and optical fiber amplifiers by this inexpensive and versatile solution-based approach.

3:00 PM - 3:20 PM (G-038-97)

THE PREDICTION OF GLASS-FORMING ABILITY, CONNECTIVITY AND RIGIDITY PERCOLATION IN CHALCOGENIDE GLASSES FROM THE PHYSICAL PROPERTY CHANGES ASSOCIATED WITH GLASS TRANSITION,

Udayan Senapati
PhD Student at New York State College of Ceramics, Alfred, NY 14802, USA

ABSTRACT

To understand the effects of average coordination number, <r>, on glass-forming capability, connectivity and rigidity percolation properties such as thermal expansion coefficient, molar volume, heat capacity, glass transition temperatures, viscosity, hardness, elastic modulus, acoustic attenuation and isothermal compressibility were studied as a function of <r> in chalcogenide glasses. In early eighties, Phillips proposed the constraint theory for covalent glasses, suggesting that ideal glass-forming condition should occur when number of constraints match the degrees of freedom. This condition is satisfied at <r> = 2.4 for covalent glasses. Most of the earlier experiments, in this field, to support Phillips' constraint theory of an existing percolation threshold at <r> = 2.4 concentrated on locating extremum behavior either in glassy state properties or in liquid state properties of chalcogenide glasses and, hence, were futile. The present work shows that the ***key to the problem of percolation threshold*** is embodied in ***configurational changes*** associated with glass transition.

3:20 PM - 3:40 PM (G-039-97)

NEGATIVE PRESSURE UPON GLASS TRANSITION,

L.M. Landa* and K.A. Landa, LANCER TECH, INC., Greensburg, PA 15601, tel. 412-623-8097

Relaxation of a glassforming liquid is accompanied by the decrease in volume and increase in entropy. Hence, the pressure in the system is negative. With the decrease of temperature in the interval $T_f > T_g > T_c$, the time of relaxation changes monotonously, while the pressure remains negative. T_c is the temperature below which the level of the heat fluctuations of density does not depend on temperature. At T_c (not at T_g !) the time of relaxation undergoes an abrupt change, with (a) or without (b) the release of the latent heat. Freezing of relaxation at T_c is, by its nature, a phase transition of the first (a) or second (b) order. This phase transition is one of the forms of relaxation rather than its alternative. Negative pressure conditions a rare (though experimentally observed in crystals) feature of a second order phase transition which is characteristic of the systems "melt-glass": the phase of a higher symmetry (glass) is a low-temperature phase compared to the phase of considerably lower symmetry (melt). This feature explains in particular, the unusual dependence of the transition temperature on the rate of cooling.

3:40 PM - 4:00 PM (G-040-97)

Evidence of transitions in "fragility" of mixed alkali glasses

P.F. Green^, R.K. Brow+ and J.J. Hudgens#, ^Dept. Chemical Engineering, The University of Texas at Austin, Austin, TX, +Sandia National Laboratories, Albuquerque, NM, #Texas Instruments, Dallas, TX.

The transition from "strong" to "fragile" behavior exhibited by glass melts is accompanied by increases in the magnitude of the heat capacity change, $\Delta C_p(T_g)$, at the calorimetric glass transition temperature, T_g. It is well documented that this transition is associated with the increasing configurational degeneracy of more ionic (non-directional) character of the molecular bonding as the alkali oxide content is increased. Our studies of a mixed alkali (Li, Na) metaphosphate system in which the total number of Na and Li ions remain fixed show that ΔC_p exhibits a minimum when the number of the Li ions is comparable to the number of Na ions. This unanticipated observation is corroborated by an independent analysis of the viscous and mechanical relaxations exhibited by these glasses. Our studies will be discussed in terms of Adams-Gibbs theory and of spectroscopic studies of the molecular structure of the system.

*This work was performed at Sandia National Laboratories and was supported by the US Department of Energy under contract number DE-AC04-95AL8500.

Room: 200 **Tuesday Afternoon, May 6**
N.J. Kreidl Award Winner

4:00 PM - 5:00 PM (G-041-97)

Sol-Gel Synthesis of Rare-Earth-Doped Lanthanum Halides For Highly Efficient 1.3 μm Optical Amplification

John Ballato,* Richard E. Riman, and Elias Snitzer

Rutgers, The State University of New Jersey, *Fiber Optic Materials Research Program*, Department of Ceramic Science & Engineering, Brett and Bowser Roads, Piscataway, NJ 08855-0909

Praseodymium- and dysprosium-doped lanthanum halide powders have been synthesized via a sol-gel/reactive atmosphere approach and their luminescent properties evaluated experimentally and theoretically. Emission at 1.3 μm was observed for the first time from a sol-gel-derived material. Measured lifetimes corresponded to radiative quantum efficiencies of approximately 8 % for Pr^{3+}:LaF_3, 41 % for Pr^{3+}:$LaCl_3$ and 78 % for Dy^{3+}:$LaCl_3$. The spectroscopic properties of these hosts are shown to be comparable to melt-grown single-crystal analogs verifying the ability of inexpensive and flexible solution-based methodologies to produce low phonon-energy materials.

9:20 AM - 9:40 AM (G-045-97)

Sol-Gel Synthesis of Multicomponent Fluorides Glasses

John Ballato,* Joel Plewa, Richard E. Riman, and Elias Snitzer
Rutgers, The State University of New Jersey, *Fiber Optic Materials Research Program*, Brett and Bowser Roads, Piscataway, NJ 08855-0909

The sol-gel synthesis of heavy-metal fluoride glasses is of technological significance owing to the versatility, ease, and low-cost of the process. Metal-organics have been shown to be ineffective precursors to the realization of high-quality fluorides due to the inability to fully remove carbonaceous species. As such, metal-inorganic precursors have been developed which do attain intrinsic performance. The synthesis of ZBA (ZrF_4 - BaF_2 - AlF_3) and ZBLA (ZrF_4 - BaF_2 - LaF_3 - AlF_3) compositions are considered in terms of precursor choice and fluorination procedures. Comparisons to conventionally-prepared analogs are made with respect to optical and thermal properties.

9:40 AM - 10:00 AM (G-047-97)

FLUORIDE FIBERS BY SOL-GEL CORE DEPOSITION, C. Haines*, J. Ballato, R.E. Riman, Fiber Optics Materials Research Program, Rutgers, The State University, Piscataway, NJ 08855-0909

The sol-gel synthesis of heavy metal fluorides has been shown to be an effective method for producing amorphous, high purity materials at a greatly reduced cost in comparison to conventional melt-quench methods. Existing methods for the synthesis of powder and monolithic sol-gel derived fluorides were extended to the fabrication of single mode optical fibers. Tubular preforms were rotational casted, internally coated with sols consisting of hydrous Zr, Ba, La, and Al, fluorinated with anhydrous HF, and drawn into fiber. Typical draw conditions resulted in undesirable asymmetric cores in the fiber. The roles of sol-gel and fiber draw processing variables will be discussed with respect to how they influence the characteristics of the fiber core.

10:00 AM - 10:20 AM (G-048-97)

NANOPOROUS GLASSES AS SEPARATION MEMBRANES, C.E. Lord* and Dr. J.E. Shelby, New York State College of Ceramics at Alfred University, Alfred, NY 14802. (607) 871-2120

Alkali borosilicate glasses have a large compositional region of phase separation consisting of a silica rich phase and a borate rich phase. The glasses can be formed with interconnected structures, allowing the borate phase to be leached from the silica phase. The porous silica glass can then be consolidated to decrease the size of the pores which causes different gas permeability rates through the glass. The glass is consolidated such that gases of different sizes can be separated. The scale of the phase separation is determined in part by the identity of the alkali ion in the original glass composition. For this study, mixed alkali borosilicate glasses were used to vary the scale of phase separation and the consolidation behavior. Glasses of composition x Li_2O (7-x) Na_2O 23 B_2O_3 70 SiO_2 and x Li_2O (10-x) Na_2O 20 B_2O_3 70 SiO_2 were studied. Results will be discussed in terms of glass composition, gas separation ratios, percent porosity, pore size distribution and surface area.

10:20 AM - 10:40 AM (G-049-97)

INFRARED TRANSMITTING GLASS-CERAMICS, B. B. Harbison*, S. S. Bayya, J. S. Sanghera, and I. D. Aggarwal, Naval Research Labs, Code 5603, Washington, DC, 20375

Gallogermanate glasses have been ceramized to produce greater physical and mechanical properties while maintaining high transmission in the 2-5 micron wavelength region. Properties including rupture strength, fracture toughness, hardness, Young's modulus and chemical durability are greatly enhanced by the ceramization process. Through careful nucleation and crystal growth heat treatments, these glass-ceramics contain crystals <500 nm in size which does not impede transmission in the near infrared. Gallogermanate glass-ceramics can be manufactured at a fraction of the cost of competing materials. These materials can find potential applications in missile domes, midwave IR windows on defense and civilian aircraft, military vehicles and automobiles.